

1 **Changes in Western Pacific Tropical Cyclones**
2 **Associated with the El Niño-Southern Oscillation**
3 **Cycle**

4
5 Richard C. Y. Li¹, Wen Zhou¹

6 ¹ *Guy Carpenter Asia-Pacific Climate Impact Centre, School of Energy and*
7 *Environment, City University of Hong Kong, Hong Kong, China*

8
9
10
11
12
13
14
15
16
17
18
19
20
21

1 **Abstract**

2 This study examines the interannual variability of three groups of tropical
3 cyclones (TCs)—super typhoons (STYs), typhoons (TYs), and tropical storms and
4 tropical depressions (TSTDs)—and their relationship with the El Niño-Southern
5 Oscillation (ENSO). Both wavelet analysis and correlation studies of upper ocean
6 heat content (OHC) reveal significant differences for the three types of TCs. In
7 particular, an increase (decrease) in the frequency of STYs is usually associated with
8 the mature phase of El Niño (La Niña) events, while the converse is true for TSTDs.
9 In contrast, the frequency of TYs increases (decreases) during the transition period
10 from La Niña to El Niño (El Niño to La Niña) events. The results suggest that the
11 timing with which ENSO impacts STYs, TYs, and TSTDs varies and that their
12 corresponding changes in frequency closely follow the evolution of the ENSO cycle.

13 Empirical orthogonal function analysis is also conducted to investigate the
14 impact of different environmental factors influenced by ENSO on TCs. The vertical
15 wind shear and moist static energy associated with ENSO are identified as the
16 dominant factors that control the frequency of STYs. In comparison, the frequency of
17 TYs is found to be closely related to the relative vorticity and vertical wind shear
18 associated with both the transition phase of ENSO and with other types of climate
19 variability.

1 **1. Introduction**

2 Over the past few decades, many studies have focused on the relationship
3 between western North Pacific (WNP) tropical cyclones (TCs) and the El Niño-
4 Southern Oscillation (ENSO; Chia and Ropelewski 2002; Wang and Chan 2002;
5 Camargo and Sobel 2005; Chan 2007; Huang and Xu 2010; Kim et al. 2011). For
6 example, Wang and Chan (2002) found that a southeastward (northwestward) shift in
7 the positions of TC genesis in the WNP occurs during El Niño (La Niña) years which
8 in turn may favor (suppress) the development of intense TCs. Camargo and Sobel
9 (2005) discovered that the accumulated cyclone energy (ACE; Bell et al. 2000) is
10 positively correlated with ENSO indices, suggesting that stronger (weaker) and
11 longer-lasting (shorter-lived) TCs tend to form during an El Niño (La Niña) event.
12 Following this, Camargo et al. (2007a and b) investigated the impacts of ENSO on the
13 tracks and genesis locations of TCs. Making use of a genesis potential index
14 (Emanuel and Nolan 2004), they suggested that vorticity and relative humidity play
15 an important role in the eastward shift in the mean genesis location of TCs in the
16 WNP. Chan (2007) also pointed out that interannual variations in intense typhoons in
17 the WNP are unlikely to be determined by local sea surface temperature (SST) but are
18 related to changes in planetary-scale atmospheric circulation (vorticity and wind shear)
19 and thermodynamic structure (moist static energy; MSE) associated with the El Niño
20 phenomenon. More recently, Huang and Xu (2010) attributed the increase in the
21 number of super typhoons (STYs) in El Niño years to changes in SST, the monsoon
22 trough, and vertical wind shear (VWS).

23 These studies focused mainly on the effect of ENSO on intense TCs (Chan
24 2007; Huang and Xu 2010) or considered all TCs as a whole regardless of their
25 intensity (Chia and Ropelewski 2002; Wang and Chan 2002; Camargo et al. 2007b;

1 Kim et al. 2011). Thus, the effect of ENSO on weaker typhoons or tropical
2 depressions is unclear, and the connection between ENSO and TCs with different
3 intensities remains uncertain. In addition, less effort on studying the TC-ENSO
4 relationship during the ENSO transition phase has been received. Frank and Young
5 (2007) recently suggested that the variance in factors that control the formation of
6 TCs can ultimately result in storms with different degrees of intensity. Thus, the
7 impact of ENSO on TCs with different intensities is also expected to vary.

8 In contrast to most ENSO-TC studies that use anomalies in SST in the Niño 3
9 or Niño 3.4 regions as a method of diagnosing the impact of ENSO, the present study
10 uses upper ocean heat content (OHC) as a proxy for ENSO, since previous studies
11 have shown that this factor also serves as an important indicator of ENSO (Kessler
12 1990; Kinter et al. 2002; Zhou and Chan 2007). Wang et al. (1999) indicated that the
13 strongest ENSO signal occurs in the subsurface as a result of wind stresses driven by
14 ENSO. However, few previous investigations have used OHC to study the impact of
15 ENSO on TCs. A recent study by Wada and Chan (2008) suggested that a decrease in
16 OHC in the WNP is related to the passage of TCs, though they did not delve deeply
17 into the relationship between OHC, ENSO, and TCs. Therefore, this study uses OHC
18 to examine the impact of ENSO on TCs with different intensities.

19 Section 2 describes the datasets used and the classification of different groups
20 of TCs. Sections 3 and 4 investigate the interannual variability of different groups of
21 TCs and their relationship with ENSO. Section 5 examines the connection of TC
22 frequency with large-scale environmental parameters. Finally, a discussion and
23 summary is given in section 6.

24 **2. Datasets and definitions**

25 The TC datasets of the WNP were obtained from the Joint Typhoon Warning

1 Center
2 (http://www.usno.navy.mil/NOOC/nmfc~ph/RSS/jtwc/best_tracks/wpindex.html),
3 which records the location and intensity of all TCs at 6-h intervals. July to November
4 (JASON) is taken to be the TC season, during which about 80% of the total number of
5 TCs in the WNP (0–30°N, 120–180°E) occur. The study period of 1965 to 2006 was
6 chosen based on the availability of routine satellite observations. TCs formed during
7 this period are categorized into one of the three groups according to their maximum
8 attainable intensity. The super typhoon (STY) group includes TCs that reach at least
9 114 knots (Cat 4 and 5 in the Saffir-Simpson Hurricane Scale), accounting for about
10 26% (223/850) of the total number of TCs and representing the most intense TCs. The
11 typhoon (TY) group comprises moderately strong TCs with a maximum sustained
12 wind speed between 64 and 114 knots (Cat 1–3 in the Saffir-Simpson Hurricane Scale)
13 and accounts for a further 37% of the total frequency (316/850). The remaining 37%,
14 with a maximum sustained wind speed of less than 64 knots (311/850), is classified as
15 the tropical storm and tropical depression (TSTD) group and corresponds to the
16 weakest type of TC.

17 Monthly atmospheric data for temperature, sea level pressure, 500 hPa omega,
18 600 hPa relative humidity, and 850 hPa and 200 hPa wind for the period 1965–2006
19 were obtained from the National Centers for Environmental Prediction-National
20 Center for Atmospheric Research (NCEP-NCAR) reanalysis (Kalnay et al. 1996). The
21 monthly National Oceanic and Atmospheric Administration (NOAA) 2° x 2° extended
22 reconstructed SST dataset (Smith and Reynolds 2004) was also used to compute the
23 Niño 3.4 index for comparison with the OHC. Monthly upper ocean temperatures for
24 depths of 0–400 m from the Scripps Institution of Oceanography of the Joint
25 Environmental Data Analysis Center for the period 1965–2003 were used to compute

1 the OHC, with standard depths of 0, 20, 40, 60, 80, 120, 160, 200, 240, 300, and 400
2 m and a horizontal resolution of $5^\circ \times 2^\circ$. Following Zhou and Chan (2007), the upper
3 OHC for the first 400 m was computed by:

$$4 \quad \text{OHC} = \int_{-h}^0 \rho C_p T dz$$

5 where C_p is the specific heat capacity at constant pressure, ρ is the density of the
6 fluid, and T is temperature of the mixed layer.

7 **3. Interannual variability of TCs in association with OHC**

8 *a. Variability of TCs with different intensities*

9 During 1965–2006, an average of 5.31 STYs, 7.52 TYs, and 7.40 TSTDs
10 formed in the WNP, with a standard deviation of 2.35, 2.70, and 2.78 respectively.
11 Figure 1 shows the corresponding standardized time series of the STY, TY, and TSTD
12 frequencies in the WNP during the TC season (JASON). Interannual as well as
13 interdecadal variations are noted for all three TC groups. However, it should be
14 pointed out that the interrelationship between these three groups of TCs is weak such
15 that no significant correlation can be revealed (Table 1). In other words, a higher
16 occurrence of a certain TC group does not necessarily imply a higher frequency of the
17 others. For example, in the period 2002–2006, a below-average number of TSTDs and
18 TYs were recorded in the WNP (Figures 1b and 1c), while more STYs were actually
19 noted during this period (Figure 1a).

20 To clearly identify the dominant modes of variability, the real-valued Mexican
21 hat wavelet, the second derivation of a Gaussian (DOG; derivative $m = 2$), was also
22 applied to the three frequency time series (Figure 2). This method has also been
23 employed in previous TC studies (Chan 2008; Chan and Xu 2009) for mode
24 identification, and further details can be found in Torrence and Compo (1998).

1 Consistent with the above weak correlations between the three TC groups, the wavelet
2 power spectra of the three groups of TCs demonstrate different features. For instance,
3 the 2–7-year signal is more prominent in the late 1990s for STYs (Figure 2a) in a way
4 similar to that in Chan (2008), whereas it appears before the 1990s in the TY
5 spectrum (Figure 2b). For the weaker TSTDs, the 2–7-year band is much smaller and
6 the 16–32-year band dominates in the 1990s (Figure 2c). The results again suggest
7 that variations exist among different groups of TCs.

8 *b. The impact of OHC on TC intensity*

9 The above wavelet spectra of different groups of TCs show differences in
10 power in the 2–7-year band. As the 2–7-year band is often linked to ENSO, the impact
11 of ENSO on different groups of TCs is also expected to vary.

12 As discussed in the introduction, OHC, rather than SST anomalies, was used as
13 a proxy for ENSO. Therefore, in order to obtain a general picture of how OHC is
14 related to ENSO, a correlation map between the Niño 3.4 SST with basinwide OHC
15 was first computed (Figure 3). The correlation pattern exhibits a distinct east-west
16 dipole in the Pacific with a significant positive (negative) correlation in the eastern
17 (western) Pacific, which is similar to the pattern found by Zhou and Chan (2007).
18 Such a pattern is consistent with the accumulation of warm water in the eastern
19 Pacific associated with El Niño events. The results here support the previous view
20 that OHC is a good indicator of ENSO (Kessler 1990; Kinter et al. 2002; Zhou and
21 Chan 2007) and is thus suitable to use in the present study.

22 To investigate the relationship with OHC and its possible linkage to ENSO, a
23 lead-lag correlation was computed for different TC intensity groups (Figures 4, 6, and
24 7), in which year 0 denotes simultaneous correlation while year -1 (+1) represents the
25 correlation when OHC leads (lags) the TC by one year. For the frequency of STYs

1 (Figure 4), the correlation is rather weak in the Pacific in year -1 and year 1, while a
 2 prominent east-west dipole pattern similar to that in Figure 3 is found in year 0. As
 3 implied by the dipole pattern between OHC and ENSO, this similar dipole pattern for
 4 OHC and STYs in year 0 suggests that the frequency of STYs might be related to
 5 ENSO in such a way that more (fewer) STYs tend to develop during an El Niño (La
 6 Niña) event. This result agrees well with previous studies (Wang and Chan 2002;
 7 Camargo and Sobel 2005; Camargo et al. 2007a) that showed that stronger and
 8 longer-lasting TCs tend to form during an El Niño event. One important point that
 9 needs to be addressed here is that the significant negative correlation in the western
 10 Pacific is mainly a response to ENSO, rather than the cooling effect due to the
 11 passage of STYs. This is confirmed by the partial correlation after removal of the
 12 ENSO effect (Figure 5), which is calculated based on the following formula:

$$r_{xy.z} = \frac{r_{xy} - (r_{xz})(r_{yz})}{\sqrt{(1 - r_{xz}^2)(1 - r_{yz}^2)}}$$

13
 14 where r is the simple correlation coefficient and the subscripts x , y , and z represent the
 15 STY frequency, the OHC, and the OHC in the Niño 3.4 region, respectively. This
 16 allows us to determine the correlation between variables x and y with the effect of z
 17 removed. In contrast to the significant negative correlation in the western Pacific
 18 shown in Figure 4b, the local correlation is greatly weakened in both magnitude and
 19 spatial extent in Figure 5, indicating that the significant negative correlation is mainly
 20 contributed by ENSO. This is consistent with previous results (Chan 2007) that
 21 showed a weak relationship between local SST (in this case the local OHC) and TCs
 22 compared with ENSO.

23 In contrast to STYs, the correlation between OHC and TYs shows different
 24 patterns (Figure 6). Instead in year 0, the correlation with an ENSO-like dipole pattern

1 appears in both year -1 and year 1, which suggests that the frequency of TYs tends to
2 increase (decrease) during the transition from La Niña to El Niño (El Niño to La Niña)
3 events. These results imply that different phases of ENSO affect STYs and TYs in
4 different ways. Modulation of STYs tends to occur during the mature phase of ENSO,
5 while that of TYs appears to be related to the transition phase. Finally, the
6 simultaneous correlation for the TSTD group (Figure 7) appears to be similar to that
7 of the STY group, although the sign in year 0 is reversed and the correlations in year -
8 1 and year 1 are weak. All of these findings imply that the timing with which ENSO
9 impacts STYs, TYs, and TSTDs differs and the corresponding changes in their
10 frequencies appear to follow the ENSO cycle closely.

11 **4. The TC-ENSO relationship**

12 To confirm the above correlation results between the frequency of different TC
13 groups and OHC, composite analysis is also carried out to illustrate the impact of
14 ENSO on different groups of TCs. The OHC anomaly composites are based on the
15 more/fewer TC years (denoted by year 0), when the JASON standardized TC
16 frequency is more/less than 1/-1 (refer to Table 2 for the selected years). In addition,
17 the evolution of OHC anomalies 2 years before and after year 0 (denoted by year -2
18 and year 2, respectively) are also shown. Figure 8a shows the longitude-time sections
19 of OHC anomaly composites along the equator for the fewer-STY case. In year -2,
20 positive (negative) OHC anomalies appear in the eastern (western) Pacific, which is
21 typical of the El Niño pattern. Accordingly, a generally higher than normal STY
22 frequency can be found during this period, which agrees well with the significant
23 positive correlation of STYs and OHC as revealed in section 3b. The negative OHC
24 anomalies in the western Pacific begin to propagate eastward in year -1. The variation
25 in the number of STYs during this period is small, while a generally below-average

1 total TC number is recorded. The negative OHC anomalies finally reach the eastern
2 Pacific in early year 0, which signifies the mature stage of the La Niña event, during
3 which the occurrence of STYs is significantly reduced. At the same time, it is also
4 interesting to note that the number of total TCs during this period is generally above
5 normal, which again suggests that the increase in total TC formation does not
6 necessarily support greater STY development. Finally, in year 1, the positive
7 anomalies in the western Pacific start to move eastward and the whole cycle is
8 repeated. The reverse is generally true for the years with a greater number of STYs, as
9 shown in Figure 8b, although the OHC anomalies and the reduction in STY number in
10 year -2 are less prominent. The above results further confirm that the frequency of
11 STYs follows the ENSO cycle, with greater (reduced) frequency during the mature
12 phase of El Niño (La Niña), while the variation in frequency is relatively smaller
13 during the transition phase. These results conform well to previous studies (Camargo
14 and Sobel 2005; Chan 2007) that found that El Niño favors the development of
15 intense TCs.

16 A similar analysis is also applied to TYs (Figure 9a). The OHC anomalies
17 depict an El Niño-like dipole pattern in year -1, indicating the mature stage of an El
18 Niño event, which differs from the case of STYs (Figure 8a). During year 0 is the
19 transition phase when the negative OHC anomalies in the western Pacific begin to
20 migrate eastward. During this period, the TY frequency shows a significant decrease,
21 which is consistent with the previous correlation result that fewer TYs will generally
22 be found during an El Niño to La Niña transition. Moreover, an above-normal TY
23 number can be observed in year -2, which is the transition phase from a La Niña to an
24 El Niño event. The reverse is also found for years with a greater frequency of TYs
25 (figure not shown), which indicates that ENSO impacts TYs mainly during transition

1 phases.

2 Finally, the pattern of OHC anomalies for the fewer TSTDs (Figure 9b) is
3 almost the reverse of that for STYs (Figure 8a), with significant reduction (increase)
4 in year 0 (-2) corresponding to the mature phase of an El Niño (La Niña) event,
5 though the OHC anomalies appear to be weaker and less organized. While for years
6 with a greater TSTD frequency, the OHC pattern is generally the reverse of that of the
7 fewer-TSTD case (figure not shown). This indicates that the weaker TSTDs generally
8 exhibit activity opposite to that of intense STYs during the mature phase of an ENSO
9 event.

10 To summarize, TCs of different intensities are modulated during different
11 phases of an ENSO cycle. In particular, the increase (decrease) in the frequency of
12 intense STYs is usually found to be associated with a mature El Niño (La Niña) event,
13 while the converse is found for the weak TSTD group. This is in agreement with
14 Camargo and Sobel (2005) and Camargo et al. (2007a). In contrast, modulation of the
15 number of TYs occurs mainly during the transition period of an ENSO cycle. The
16 results here suggest that weak and intense TCs could respond differently to external
17 forcing induced by an ENSO event, which will be discussed in detail in section 5.

18 As an extension, we also investigate other TC parameters, including genesis
19 position, TC lifetime, and ACE in order to achieve a more comprehensive
20 understanding of the interannual variability of TCs in the WNP. Differences in these
21 parameters between the high and low occurrence years are considered to be
22 significant when exceeding 95% confidence based on the Student's *t* test. Figure 10
23 shows the genesis positions of STYs in the WNP during the high and low occurrence
24 years. The average number of STYs formed in the high occurrence years is 8.75,
25 which is about 5.5 times greater than that in the low occurrence years (1.6), while the

1 total TC number remains approximately the same (22.1 versus 21). In addition to the
2 number of STYs generated, another noticeable feature is the difference in the genesis
3 positions, whereby the TCs formed in the years with a higher occurrence of STYs
4 exhibit a clear shift to the southeast (140–180°E, 0–15°N). In fact, such a shift in
5 genesis positions is closely related to changes in atmospheric circulation influenced
6 by ENSO (refer to section 5). Consistent with previous studies (Chia and Ropelewski
7 2002; Wang and Chan 2002; Camargo and Sobel 2005; Camargo et al. 2007a), the
8 increase in the number of STYs, together with the southeastward shift in genesis
9 positions, results in TCs with a much longer lifespan and contributes to a significant
10 increase in ACE in high occurrence years (Table 3).

11 With regard to TYs, the average number recorded in the high occurrence years
12 is 11.25, compared with 3.2 in the years with a lower occurrence, which also
13 contributes to a significant difference in total TC number during the two periods
14 (22.75 versus 15.8). In contrast to STYs, no prominent shift in the genesis position
15 (Figure 11) or changes in lifespan (Table 3) can be observed. This means that the
16 significant increase in ACE is mainly associated with an increase in the number of
17 TYs during high occurrence years. Finally, for the TSTD group (Figure 12), the
18 significant change in their number (11.9 versus 3.25) in the high and low occurrence
19 years does not lead to a prominent difference in ACE. This is because ACE is mainly
20 dominated by intense TCs, while weak TSTDs make only a minor contribution (Bell
21 et al. 2000). Indeed, the average TC lifespan in the low occurrence years is longer
22 than that in the high occurrence years which contributes to the overall larger ACE.
23 Nevertheless, the results here indicate that in addition to the genesis numbers, the
24 shifts in genesis position and the changes in mean lifespan, at least in the case of
25 intense STYs, may also be associated with ENSO. This is consistent with previous

1 studies (Chia and Ropelewski 2002; Wang and Chan 2002; Camargo and Sobel 2005;
2 Camargo et al. 2007a) in which the southeastward shift in genesis positions favored
3 the development of more intense and longer-lived TCs in El Niño years.

4 **5. Impact of large-scale environmental parameters on TC activity**

5 In the previous section, the change in frequency of different TC intensity
6 groups is found to be related to different phases of ENSO events. Therefore, ENSO
7 must exert its impact on TC activity through differences in the modulation of large-
8 scale environmental parameters. In this section, the six TC-related parameters
9 suggested by Gray (1979) are investigated, including four dynamic parameters (850
10 hPa relative vorticity, 200–850 hPa total VWS, 200 hPa divergence, and 500 hPa
11 omega) and two thermodynamic parameters (600 hPa relative humidity and 1000–500
12 hPa average moist static energy [MSE]). Following the method of Chan and Liu
13 (2004), empirical orthogonal function (EOF) analysis is first applied to the
14 standardized time series of the different parameters during the TC season.
15 Correlations are then computed for the principal component (PC) time series of each
16 mode with the Pacific dipole index (PDI) and the TC frequency. The correlation
17 results are summarized in Table 4 and Table 5, respectively. Similar to Zhou and Chan
18 (2007), the PDI is defined as the difference in OHC averaged over the eastern region
19 (110–150°W, 6°S–4°N) minus the western region (130–170°E, 0–10°N) to reflect the
20 dipole pattern during an ENSO event. Thus, a large positive (negative) value of the
21 PDI corresponds to the warm (cold) phase of ENSO. This was shown previously
22 (Zhou and Chan 2007) to be a good index to represent ENSO, with a correlation of
23 0.91 (over 99% confidence) with the Niño 3.4 index in this case. Finally, stepwise
24 regressions are performed to determine the relative contribution of each
25 environmental parameter to the prediction of TC frequency.

1 *a. Dynamic factors*

2 EOF1 of the low-level relative vorticity reveals a north-south dipole pattern
3 (Figure 13), with a maximum positive center situated in the southeastern part of the
4 western Pacific. Such a pattern is consistent with that found by Chan and Liu (2004)
5 and explains 22.4% of the total variance. This represents the interannual variability of
6 the strength of the monsoon trough in the WNP. The corresponding PC time series
7 reveals a significant positive (negative) correlation of 0.34 (-0.36) at 95% confidence
8 with the STY (TSTD), while it correlates only weakly with the TY frequency (0.076).
9 At the same time, the PC time series shows a significant positive correlation (0.85 at
10 99% confidence) with the PDI, indicating that it is closely linked to ENSO. The
11 importance of monsoon trough and relative vorticity associated with the eastward
12 shift in the mean genesis location has also been mentioned in previous studies (Wu et
13 al. 2004; Camargo et al. 2007a and b; Kim et al. 2011). Consistently, the EOF1
14 pattern here suggests that an increase in low-level relative vorticity, with a maximum
15 in the southeast region associated with the strengthening of the monsoon trough,
16 favors (suppresses) the formation of intense STYs (weaker TSTDs) during an El Niño
17 event.

18 In contrast, the PC time series of EOF2 depicts a much more significant
19 correlation with TY frequency (0.33 at 95% confidence) compared with that of STY
20 (0.24) and TSTD (0.12). The positive center migrates northward to about 155°E,
21 20°N. This pattern was not discussed by Chan and Liu (2004). Instead of showing
22 significant simultaneous correlations, the time series of PC2 reveals a significant lag-
23 1 correlation (-0.30 at 90% confidence) as well as a lead-1 correlation (0.26 at 90%
24 confidence) with the PDI. This suggests that a positive (negative) EOF2 pattern
25 usually occurs during La Niña to El Niño (El Niño to La Niña) transitions, which in

1 turn affects the formation of TYs. Therefore, a change in the number of TYs during
2 the transition phase, as revealed in the previous section, can be attributed partly to a
3 concomitant change in low-level vorticity induced by ENSO.

4 The first EOF of the total VWS shows an alternating pattern, with a positive-
5 negative-positive orientation (Figure 14). This pattern is found to be significantly
6 correlated only with STY frequency (0.31 at 95% confidence), while at the same time
7 being closely linked to the PDI (0.64 at 99% confidence). This implies that a weaker
8 wind shear in the southeast (165–180°E, 5–15°N) during an El Niño event is
9 particularly favorable for STY development, even though a higher than normal value
10 appears in the western region. The pattern is consistent with that in Camargo (2007b)
11 and Kim et al. (2011), who have similarly found a reduction in shear near the dateline
12 during El Niño years.

13 Although the time series of PC2 is found to be significantly correlated with the
14 frequency of TYs (-0.46 at 99% confidence), it reveals no significant relationship with
15 the PDI. This suggests that the significant impact of EOF2 on TY frequency is related
16 to factors other than ENSO. This may be due to a weaker ENSO forcing during the
17 transition phase compared with the mature phase, such that other types of climate
18 variability may also play a role in affecting the number of TYs. However,
19 determination of the exact nature of this climate variability is beyond the scope of this
20 study and requires future investigation.

21 With regard to midlevel vertical motion (Figure 15), only the EOF2 mode with
22 a southeast-northwest dipole pattern reveals a significant correlation with the
23 frequency of STYs, while EOF1 does not show any significant relationship with any
24 of the TC groups. In addition, the time series of PC2 also correlates positively with
25 the simultaneous PDI (0.71 at 99% confidence). This suggests that an anomalous

1 rising motion (denoted by the negative center) in the southeast region during an El
2 Niño event favors the formation of STYs. Such a change in vertical motion is also
3 consistent with the strengthening of the monsoon trough, which results in a stronger
4 cyclonic inflow at low levels during an El Niño event, as discussed in Figure 13.

5 The first EOF of 200 hPa divergence reveals a north-south dipole pattern
6 (Figure 16). Although the time series of PC1 correlates positively (0.71 at 99%
7 confidence) with the PDI, it shows no significant relationship with the frequency of
8 different groups of TCs. This means that the upper-level divergence induced by
9 ENSO plays a relatively minor role compared with other dynamic factors. In contrast,
10 the time series of PC2 shows a significant correlation with TY frequency but reveals
11 no significant relationship with the PDI. Similar to the EOF2 of the VWS, the results
12 here suggest that the change in TY frequency through modulation of the 200 hPa
13 divergence is related to factors other than ENSO.

14 *b. Thermodynamic factors*

15 EOF1 of the 600 hPa relative humidity again shows a southeast-northwest
16 dipole pattern (Figure 17). The correlations with both STY frequency (0.58 at 99%
17 confidence) and the PDI (0.52 at 99% confidence) are significantly positive. This
18 means that an increase in midlevel relative humidity in the southeast region during an
19 El Niño event is beneficial for the development of STYs. Our results here agree with
20 previous studies (Camargo et al. 2007b; Kim et al. 2011), which reveal a similar
21 increase in humidity near the dateline during an El Niño event. On the contrary, EOF2
22 shows no significant relationship with different TC parameters, though PC2 reveals a
23 significant lag-1 correlation (-0.31 at 90% confidence) with the PDI.

24 Finally, for the MSE (Figure 18), only EOF2 is found to be related to the
25 number of both STYs (0.55 at 99% confidence) and TSTDs (-0.26 at 90% confidence),

1 while EOF1 is not. Again, EOF2 reveals a southeast-northwest dipole pattern with a
2 significant positive correlation of 0.72 with the PDI, which implies that an increase in
3 MSE in the southeast region would result in an increase (decrease) in the number of
4 STYs (TSTDs) during an El Niño event. Such a pattern also resembles the EOF2
5 pattern of MSE obtained by Chan and Liu (2004), which further supports our results.

6 *c. Stepwise regression*

7 As an extension of Chan and Liu (2004), this section investigates how different
8 dynamic and thermodynamic factors are related to TCs with different intensities and
9 how they are linked to different phases of ENSO. As shown in Tables 4 and 5, the PC
10 time series (including 850 hPa relative vorticity, VWS, 500 hPa omega, 600 hPa
11 relative humidity, and average MSE), which shows significant correlations with STY
12 frequency, is simultaneously related to the PDI. This suggests that the modulation of
13 STY frequency takes place mainly during mature ENSO events. The enhanced low-
14 level relative vorticity, midlevel rising motion, weaker VWS, and higher midlevel
15 relative humidity and MSE in the southeast quadrant during an El Niño event strongly
16 favor the development of STYs. This is consistent with the strengthening and
17 southeastward extension of the monsoon trough during an El Niño event (Wang and
18 Chan 2002; Chen and Huang 2008), which results in a southeastward shift in the TC
19 genesis position and thereby allows more time for TCs to stay over the open ocean
20 and intensify. Finally, in order to identify the relative contribution of these different
21 environmental parameters to the frequency of STYs, stepwise regression is carried out.
22 This is a systematic method for adding and removing terms from a multi-linear model
23 based on the p -values of the F -statistics so as to minimize root-mean-square error. In
24 each step, the term with the smallest (largest) p -values less (greater) than 0.05 will be
25 added to (removed from) the model. The process terminates when no additional term

1 can be added or removed from the model. The corresponding regression equation for
2 STY frequency is as follows:

3 $STY = 6.3180 - 0.1356 * VWS1 + 0.3619 * MSE2$ (with multiple R = 0.65 at 99%
4 confidence)

5 where VWS1 is the EOF1 mode for VWS and MSE2 is the EOF2 mode for MSE.
6 This suggests that wind shear and MSE play a much more critical role in predicting
7 the frequency of STYs during the mature phase of ENSO, which is consistent with the
8 results of Chan and Liu (2004).

9 TY frequency is found to be related to low-level relative vorticity, VWS, and
10 upper-level divergence, which means that dynamic factors play a much more
11 important role than thermodynamic factors in TY modulation. The change in relative
12 vorticity is found to be related to the transition phase of ENSO, while the change in
13 VWS and divergence might be related to other climate variability. Thus, during the
14 ENSO transition phase, both ENSO and other climate variability play a role in
15 regulating the frequency of TYs, which makes the situation much more complex than
16 it is for STYs. The corresponding stepwise regression equation for TY frequency is
17 given as:

18 $TY = 7.5238 + 0.1241 * RV2 - 0.1596 * VWS2$ (with multiple R = 0.54 at 99%
19 confidence)

20 where RV2 and VWS2 denote the EOF2 mode of 850 hPa relative vorticity and VWS,
21 respectively. In contrast to STY, which is controlled by both dynamic (VWS) and
22 thermodynamic (MSE) factors, TY is controlled solely by dynamic factors. This
23 extends the results of previous studies (Wang and Chan 2002; Chan and Liu 2004)
24 and further stresses the difference between factors which affect the frequencies of
25 STYs and TYs.

1 Finally, a significant relationship can also be found between the frequency of
2 TSTDs, low-level relative vorticity, and MSE associated with the mature phase of
3 ENSO. The stepwise regression equation for TSTD frequency includes only the
4 vorticity term, again emphasizing the importance of the dynamic factor in predictions
5 of weaker TCs.

6
$$\text{TSTD} = 7.4048 - 0.1258 \cdot \text{RV1} \text{ (with } R = 0.36 \text{ at 99\% confidence)}$$

7 where RV1 is the EOF1 mode of the relative vorticity.

8 **6. Summary and discussion**

9 This study examines the interannual variability of three groups of TCs—intense
10 STYs, moderately strong TYs, and weak TSTDs—and their relationship with ENSO.
11 In contrast to many previous studies, we use OHC instead of SST as a proxy for the
12 ENSO signal to determine the subsurface oceanic response to both ENSO and TCs.

13 Both wavelet analysis and correlation studies reveal significant differences
14 among the three groups of TCs. Specifically, the simultaneous correlation of OHC
15 with STYs and TSTDs depicts a significant ENSO-like dipole pattern, while that with
16 TYs does not. In contrast, the lead-1 and lag-1 correlation of OHC with TYs does
17 reveal a similar ENSO-like dipole pattern. The results suggest that the timing with
18 which ENSO impacts STYs, TYs, and TSTDs differs and the corresponding changes
19 in their frequencies closely follows the evolution of an ENSO cycle. This is further
20 supported by the composite analysis. The increase (decrease) in STY frequency in
21 more (fewer) STY years is usually associated with the mature phase of El Niño (La
22 Niña) events, while the opposite is found for TSTDs. In contrast, the frequency of
23 TYs shows an increase (decrease) during the transition period from La Niña to El
24 Niño (El Niño to La Niña). All of these findings provide new insight into the ENSO-
25 TC relationship and extend the results of previous studies (Chia and Ropelewski,

1 2002; Wang and Chan 2002; Kim et al. 2011).

2 To examine how the frequency of different groups of TCs is related to various
3 types of environmental forcing, EOF analysis is also performed. The EOF patterns of
4 the environmental factors associated with ENSO, including relative vorticity, omega,
5 relative humidity, and MSE, reveal a prominent southeast-northwest dipole pattern.
6 The enhanced low-level cyclonic vorticity, midlevel vertical motion, relative humidity,
7 and MSE as well as weaker VWS in the southeast part of the WNP provide favorable
8 conditions for STY development during El Niño years, while unfavorable conditions
9 in the northwest suppress the formation of TSTDs. These results are consistent with
10 previous studies (Chia and Ropelewski 2002; Wang and Chan 2002; Chan and Liu
11 2004; Wu et al. 2004; Camargo et al. 2007a) that showed that the strengthening of the
12 monsoon trough during an El Niño year causes a southeastward shift in the TC
13 genesis position, which in turn favors the development of intense TCs. Stepwise
14 regression emphasizes the importance of VWS and MSE (both are correlated
15 significantly with the PDI) in the prediction of the frequency of STYs, while the
16 frequency of TSTDs is found to be related largely to low-level relative vorticity.

17 On the other hand, TY frequency is found to be related to low-level relative
18 vorticity, VWS, and upper-level divergence. However, only the change in relative
19 vorticity is found to be related to the transition phase of ENSO, while the change in
20 VWS and divergence might be related to other factors. This may be due to weaker
21 ENSO forcing during the transition phase, which implies that other climate variability
22 might also contribute to the variability of TYs. Using stepwise regression, only
23 relative vorticity and VWS are identified as dominant factors that control TY
24 frequency, highlighting the importance of these two factors in forecasting TYs.

25 In a recent study, Du et al. (2011) found that VWS increases in the summer

1 following strong El Niño events through the development of a warm Kelvin wave
2 from the tropical Indian Ocean which then suppresses TC formation. Thus, the EOF2
3 pattern of VWS might be induced by forcing from the Indian Ocean, which requires
4 further investigation. In addition, Zhan et al. (2011) also suggested that the SST
5 anomaly in the East Indian Ocean (EIO; 10°S–22.5°N, 75°–100°E) affects the
6 basinwide genesis of TCs in the WNP (which also included the South China Sea
7 [SCS]). As a comparison, we also determined whether the frequency of different TC
8 groups is related to the EIO OHC. As shown by the correlation maps of OHC with
9 different TC groups (Figures 4, 6, and 7), the correlation in the EIO is not prominent
10 in most cases, which indicates that the impact of EIO OHC on TCs is generally weak.
11 The only exception is the simultaneous TY-OHC correlation, with a significant
12 negative value of -0.35 at 95% confidence, suggesting that a warming in the EIO will
13 lead to a decrease in the number of TYs in the WNP. This is consistent with the results
14 of Zhan et al. (2011), although the correlation coefficient in the present study is much
15 smaller (-0.69 in the case of Zhan et al. 2011). This discrepancy may be related to the
16 chosen study region. Zhan et al. (2011) took into account all the TCs that formed
17 within the WNP as well as the SCS, whereas we consider only those formed within
18 the WNP. This suggests that the impact of anomalous warming in the EIO on TC
19 genesis in the WNP and SCS may be different. Thus, the interaction between EIO
20 warming and ENSO on cyclogenesis in the WNP and SCS, especially during the
21 transition phase of ENSO, still requires future investigation. Nevertheless, the results
22 from this study clearly demonstrate that TCs with different intensities are modulated
23 differently by dynamic and thermodynamic factors during the various phases of
24 ENSO.

25

1 *Acknowledgment.* The research described in this paper was supported by the City
2 University of Hong Kong Croucher Foundation Grant (9220055). The authors are
3 grateful to the two reviewers and the editor for their constructive comments and
4 suggestions.
5

References

- Bell, G. D., M. S. Halpert, R. C. Schnell, R. W. Higgins, J. Lawrimore, and co-authors, 2000: Climate assessment for 1999. *Bull. Amer. Meteor. Soc.*, **81**, S1–S50.
- Camargo, S. J., and A. H. Sobel, 2005: Western North Pacific tropical cyclone intensity and ENSO. *J. Climate*, **18**, 2996–3006.
- Camargo, S. J., A. W. Robertson, S. J. Gaffney, P. Smyth, and M. Ghil, 2007a: Cluster analysis of typhoon tracks: Part II: Large-scale circulation and ENSO. *J. Climate*, **20**, 3654–3676.
- Camargo, S. J., K. A. Emanuel, and A. H. Sobel, 2007b: Use of a genesis potential index to diagnose ENSO effects on tropical cyclone genesis. *J. Climate*, **20**, 4819–4834.
- Chan, J. C. L., and K. S. Liu, 2004: Global warming and western North Pacific typhoon activity from an observational perspective. *J. Climate*, **17**, 4590–4602.
- Chan, J. C. L., 2007: Interannual variations of intense typhoon activity. *Tellus A*, **59**, 455–460.
- Chan, J. C. L., 2008: Decadal variations of intense typhoon occurrence in the western North Pacific. *Proc. R. Soc. A*, **464**, 249–272.
- Chan, J. C. L., and M. Xu, 2009: Inter-annual and inter-decadal variations of landfalling tropical cyclones in East Asia. Part I: Time-series analysis. *Int. J. Climatol.*, **29**, 1285–1293.
- Chen, G. H., and R. H. Huang, 2008: Influence of monsoon over the warm pool on interannual variation on tropical cyclone activity over the western North Pacific. *Adv. Atmos. Sci.*, **25**, 319–328.
- Chia, H. H., and C. F. Ropelewski, 2002: The interannual variability in the genesis location of tropical cyclones in the northwest Pacific. *J. Climate*, **15**, 2934–2944.
- Du, Y., L. Yang, and S.-P. Xie, 2011: Tropical Indian Ocean influence on northwest Pacific tropical cyclones in summer following strong El Niño*. *J. Climate*, **24**, 315–322.
- Emanuel, K. A., and D. Nolan, 2004: Tropical cyclone activity and the global climate system. Preprints, *26th Conf. on Hurricanes and Tropical Meteorology*, Miami, FL, Amer. Meteor. Soc., CD-ROM, 10A.2.
- Frank, W. M., and G. S. Young, 2007: The interannual variability of tropical cyclones. *Mon. Weather Rev.*, **135**, 3587–3598.
- Gray, W. M., 1979: Hurricanes: Their formation, structure and likely role in the tropical circulation. *Meteorology over the Tropical Oceans*, D. B. Shaw, Ed., Royal Meteorological Society, 155–218.
- Huang, F., and S. Xu, 2010: Super typhoon activity over the western North Pacific and its relationship with ENSO. *Journal of Ocean University of China*, **9**, 123–128.
- Kalnay, E., and coauthors, 1996: The NCEP/NCAR 40-year reanalysis project. *Bull. Am. Meteorol. Soc.*, **77**, 437–471.
- Kessler, W. S., 1990: Observations of long Rossby waves in the northern tropical Pacific. *J. Geophys. Res.*, **95**, 5183–5217.

- Kim, H.-M., P. J. Webster, and J. A. Curry, 2011: Modulation of North Pacific tropical cyclone activity by three phases of ENSO. *J. Climate*, **24**, 1839–1849.
- Kinter, J. L., K. Miyakoda, and S. Yang, 2002: Recent change in the connection from the Asian monsoon to ENSO. *J. Climate*, **15**, 1203–1215.
- Smith, T. M., and R. W. Reynolds, 2004: Improved extended reconstruction of SST (1854–1997). *J. Climate*, **17**, 2466–2477.
- Torrence, C., and G. P. Compo, 1998: A practical guide to wavelet analysis. *Bull. Am. Meteorol. Soc.*, **79**, 61–78.
- Wada, A., and J. C. L. Chan, 2008: Relationship between typhoon activity and upper ocean heat content. *Geophys. Res. Lett.*, **36**, L17603, doi: 10.1029/2008GL035129.
- Wang, B., R. Wu, and R. Lukas, 1999: Roles of the western North Pacific wind variation in thermocline adjustment and ENSO phase transition. *J. Meteorol. Soc. Japan*, **77**, 1–16.
- Wang, B., and J. C. L. Chan, 2002: How strong ENSO events affect tropical storm activity over the western North Pacific*. *J. Climate*, **15**, 1643–1658.
- Wu, M. C., W. L. Chang, and W. M. Leung, 2004: Impacts of El Niño-Southern Oscillation events on tropical cyclone landfalling activity in the western North Pacific. *J. Climate*, **17**, 1419–1428.
- Zhan, R., Y. Wang, and X. Lei, 2011: Contributions of ENSO and East Indian Ocean SSTA to the interannual variability of northwest Pacific tropical cyclone frequency*. *J. Climate*, **24**, 509–521.
- Zhou, W., and J. C. L. Chan, 2007: ENSO and South China Sea summer monsoon onset. *Int. J. Climatol.*, **27**, 157–167.

Figure captions

Figure 1: Standardized time series of JASON (a) STY, (b) TY, and (c) TSTD frequencies in the period 1965–2006. For each TC group, the standardized time series is calculated by first removing the mean and then dividing the resultant deviations from the mean by the standard deviation. The means (standard deviations) are 5.31 (2.35), 7.53 (2.70), and 7.40 (2.78) for STY, TY, and TSTD, respectively. The dotted line denotes the 10-year running mean of the standardized time series.

Figure 2: The normalized wavelet power spectrum of JASON (a) STY, (b) TY, and (c) TSTD frequency over the period 1965–2006. The cross-hatched region represents the cone of influence and the thick solid line denotes values that are over 95% confidence.

Figure 3: Correlation between Niño 3.4 SST and OHC in JASON for the period 1965–2003. The contour represents values over 95% confidence.

Figure 4: Correlation between OHC and STY frequency: (a) OHC leads STY by one year, (b) simultaneous correlation, and (c) OHC lags STY by one year during JASON for the period 1965–2003. The contour represents values over 95% confidence.

Figure 5: Simultaneous partial correlation between OHC and STY frequency during JASON for the period 1965–2003 after removal of the ENSO effect. The contour represents values over 95% confidence.

Figure 6: Same as Figure 4, except for the correlation between OHC and TY frequency.

Figure 7: Same as Figure 4, except for the correlation between OHC and TSTD frequency.

Figure 8: Longitude-time section of OHC anomaly composites (10^8 Jm^{-2}) averaged over 5S–5N for (a) fewer STY years and (b) more STY years, where year 0 refers to the less and more STY years, respectively, and year $-n$ (n) refers to n years before (after) year 0. The red (black) line on the right represents the standardized frequencies of STYs (total TCs) during the composite years.

Figure 9: Same as Figure 8, except for (a) fewer TY years and (b) fewer TSTD years. The red line on the right represents the standardized frequencies of TYs and TSTDs, respectively, during the composite years, while the black line denotes the total TC frequency.

Figure 10: Composite distribution of TCs in (a) more STY and (b) fewer STY years. The black dots represent STY genesis positions while the triangles represent genesis positions other than STY. The numbers within the parentheses indicate the number of total TCs and STYs, respectively, formed during the composite years.

Figure 11: Same as Figure 10, except for (a) more TY and (b) fewer TY years. The black dots represent TY genesis positions while the triangles represent genesis positions other than TY. The numbers within the parentheses indicate the number of total TCs and TYs, respectively, formed during the composite years.

Figure 12: Same as Figure 10, except for (a) more TSTD and (b) fewer TSTD years. The black dots represent TSTD genesis positions while the triangles represent genesis positions other than TSTD. The numbers within the parentheses indicate the number of total TCs and TSTDs, respectively, formed during the composite years.

Figure 13: EOF1 (upper panel) and EOF2 (lower panel) of the JASON mean 850 hPa relative vorticity. The sign of the EOF is chosen such that the simultaneous correlation is positive between the PC time series with the PDI. The value in the top right corner indicates the percentage of the total variance explained by each mode.

Figure 14: Same as Figure 13, except for the EOF1 (upper panel) and EOF2 (lower panel) of the total vertical wind shear.

Figure 15: Same as Figure 13, except for the EOF1 (upper panel) and EOF2 (lower panel) of the 500 hPa omega.

Figure 16: Same as Figure 13, except for the EOF1 (upper panel) and EOF2 (lower panel) of the 200 hPa divergence.

Figure 17: Same as Figure 13, except for the EOF1 (upper panel) and EOF2 (lower panel) of the 600 hPa relative humidity.

Figure 18: Same as Figure 13, except for the EOF1 (upper panel) and EOF2 (lower panel) of the 1000–500 hPa average moist static energy.

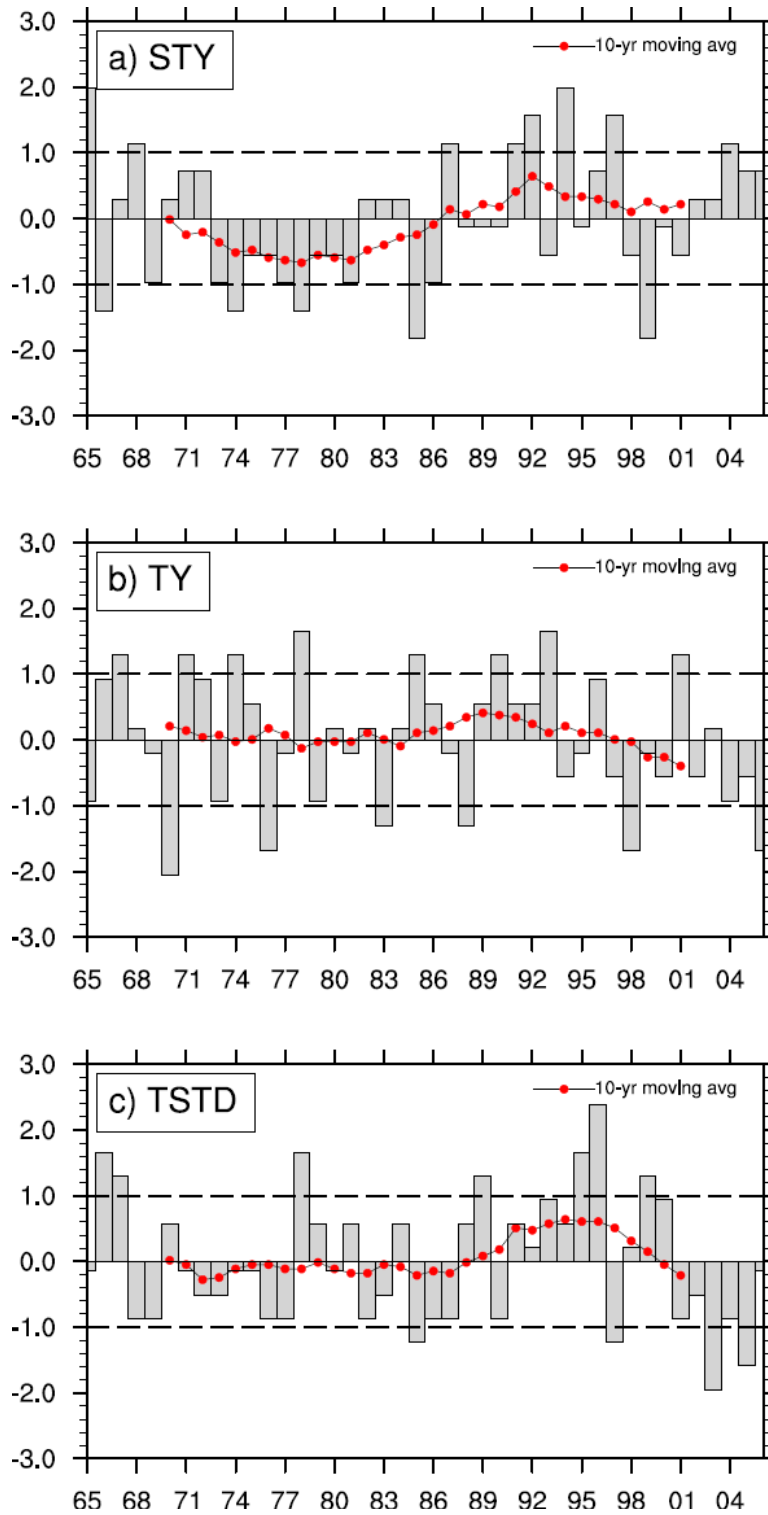


Figure 1: Standardized time series of JASON (a) STY, (b) TY, and (c) TSTD frequencies in the period 1965–2006. For each TC group, the standardized time series is calculated by first removing the mean and then dividing the resultant deviations from the mean by the standard deviation. The means (standard deviations) are 5.31 (2.35), 7.53 (2.70), and 7.40 (2.78) for STY, TY, and TSTD, respectively. The dotted line denotes the 10-year running mean of the standardized time series.

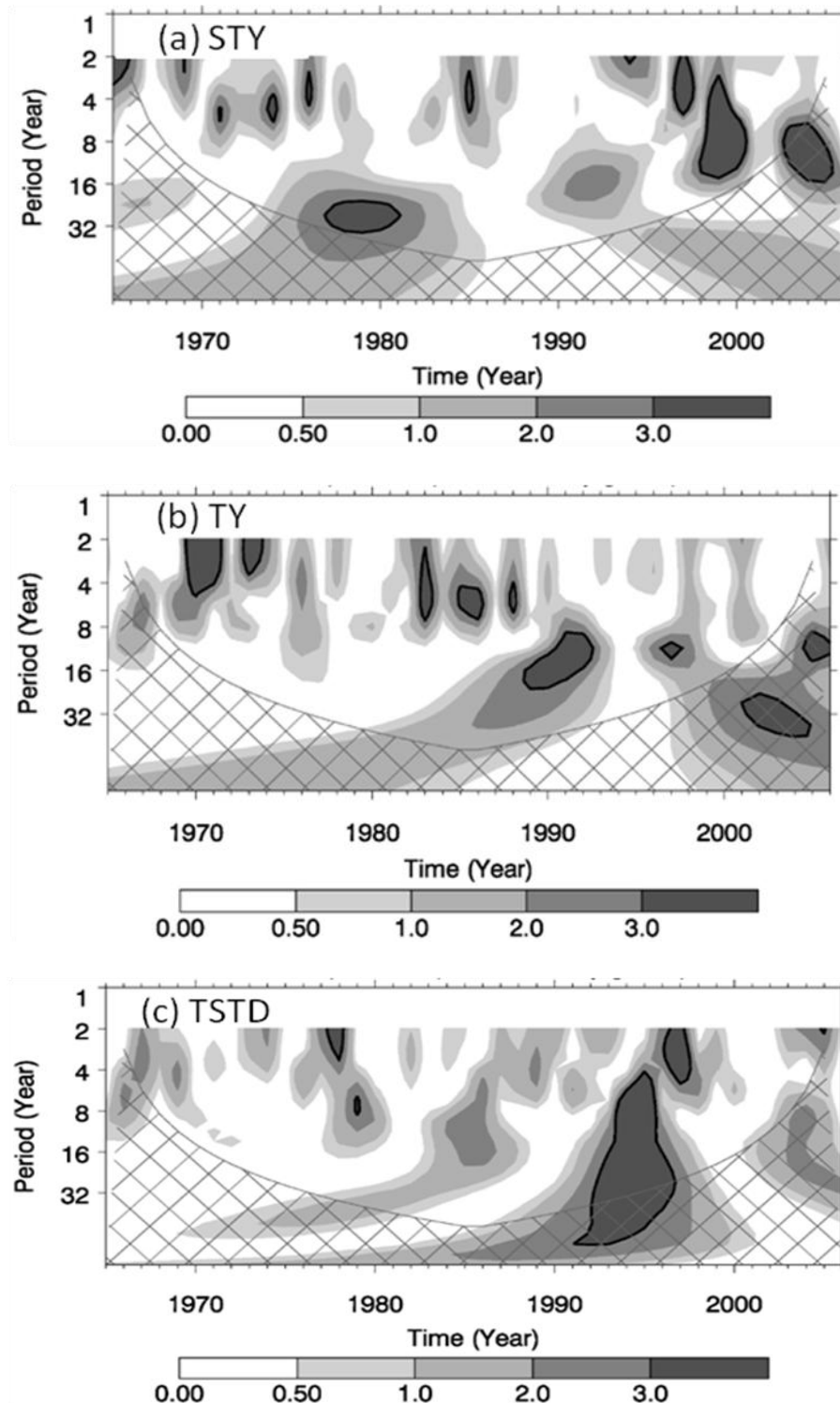


Figure 2: The normalized wavelet power spectrum of JASON (a) STY, (b) TY, and (c) TSTD frequency over the period 1965–2006. The cross-hatched region represents the cone of influence and the thick solid line denotes values that are over 95% confidence.

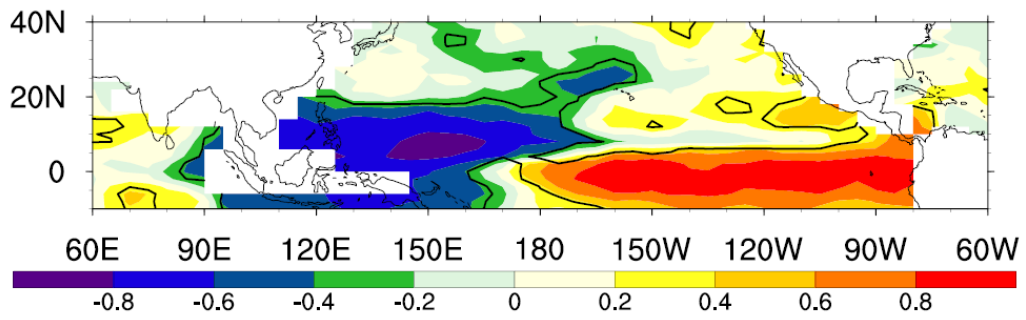


Figure 3: Correlation between Niño 3.4 SST and OHC in JASON for the period 1965–2003. The contour represents values over 95% confidence.

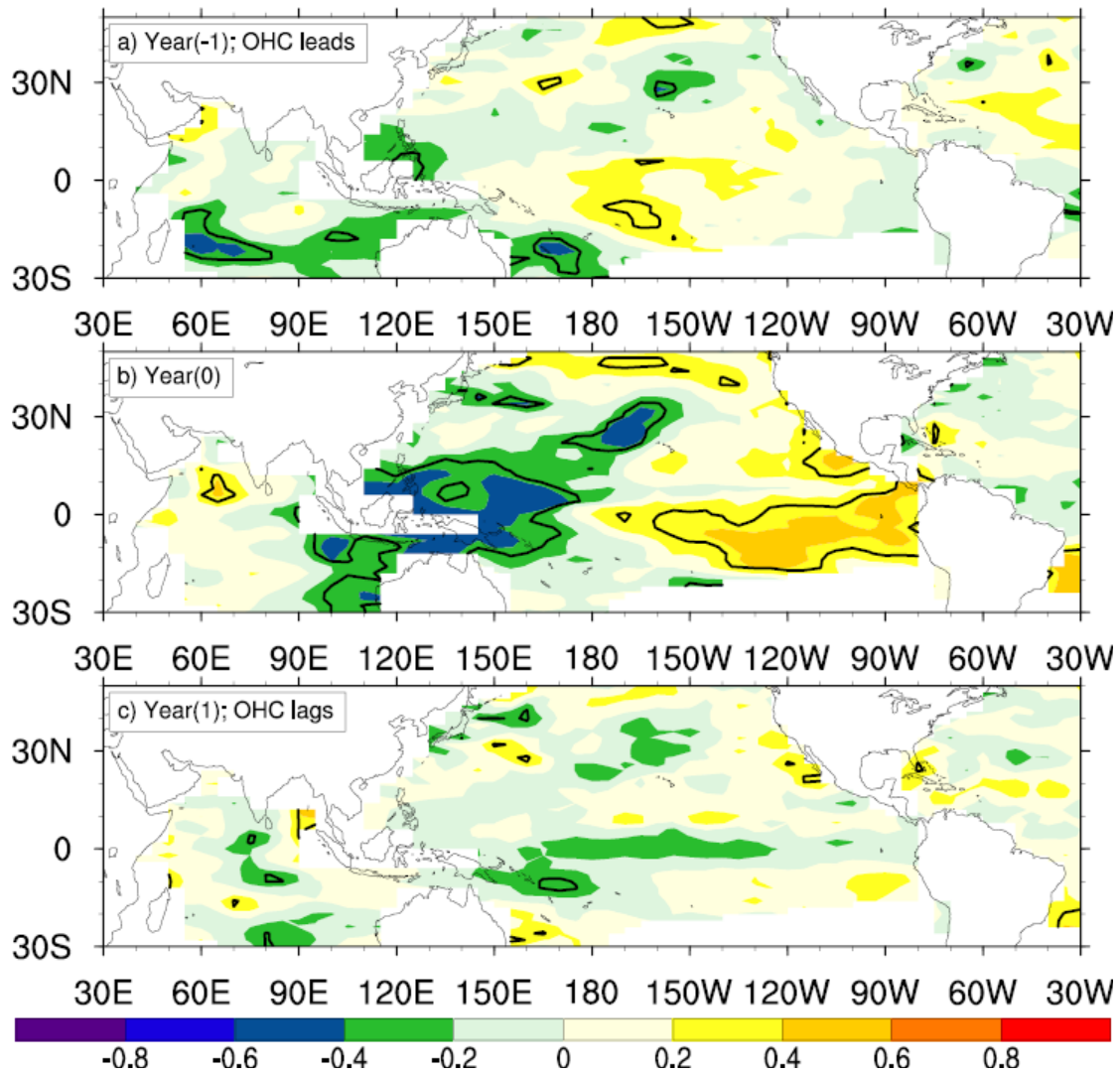


Figure 4: Correlation between OHC and STY frequency: (a) OHC leads STY by one year, (b) simultaneous correlation, and (c) OHC lags STY by one year during JASON for the period 1965–2003. The contour represents values over 95% confidence.

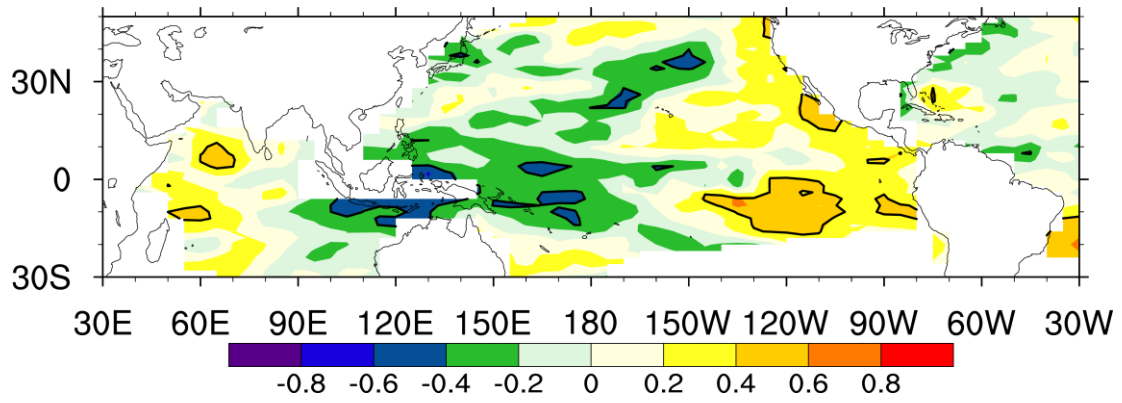


Figure 5: Simultaneous partial correlation between OHC and STY frequency during JASON for the period 1965–2003 after removal of the ENSO effect. The contour represents values over 95% confidence.

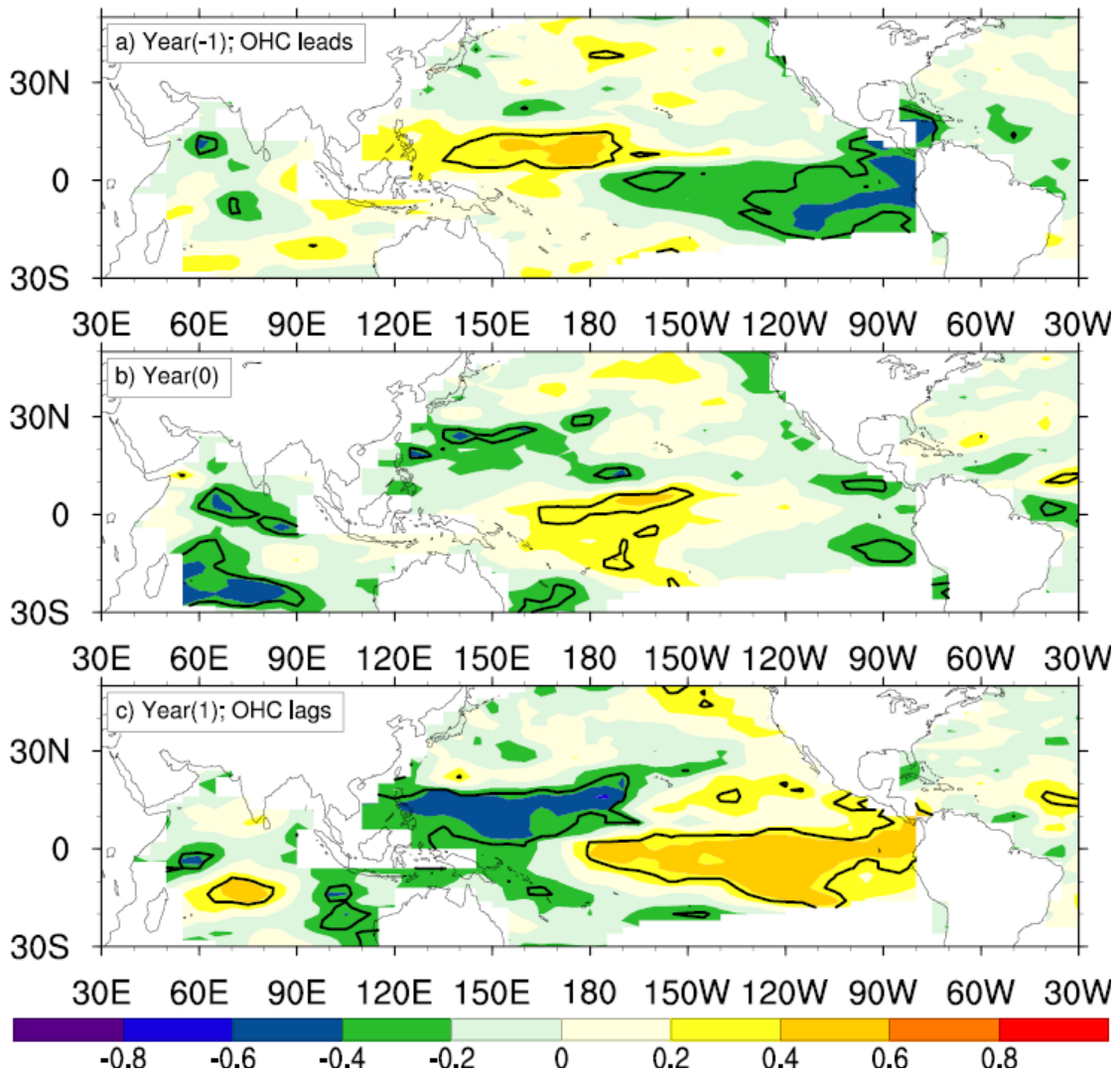


Figure 6: Same as Figure 4, except for the correlation between OHC and TY frequency.

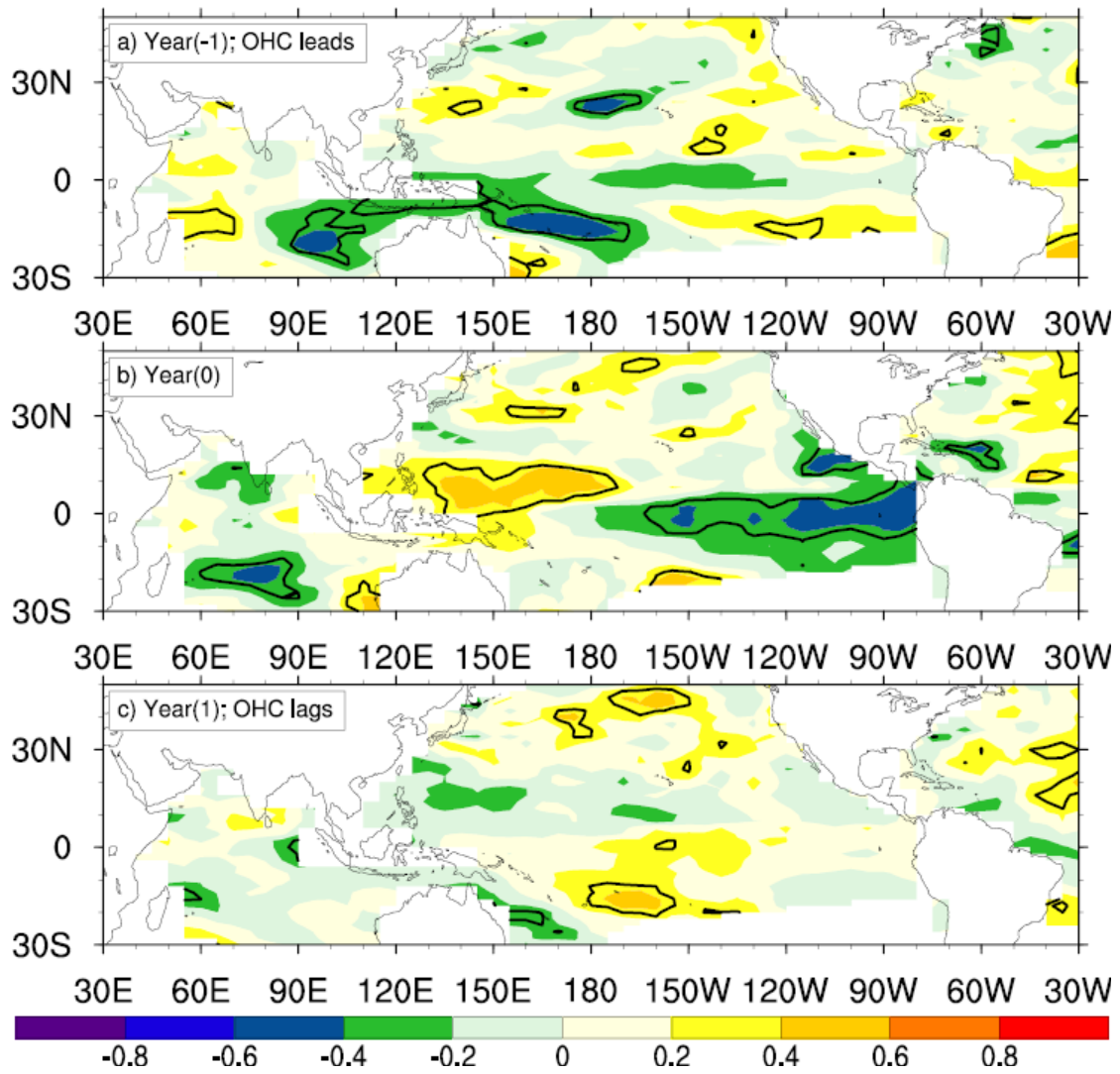


Figure 7: Same as Figure 4, except for the correlation between OHC and TSTD frequency.

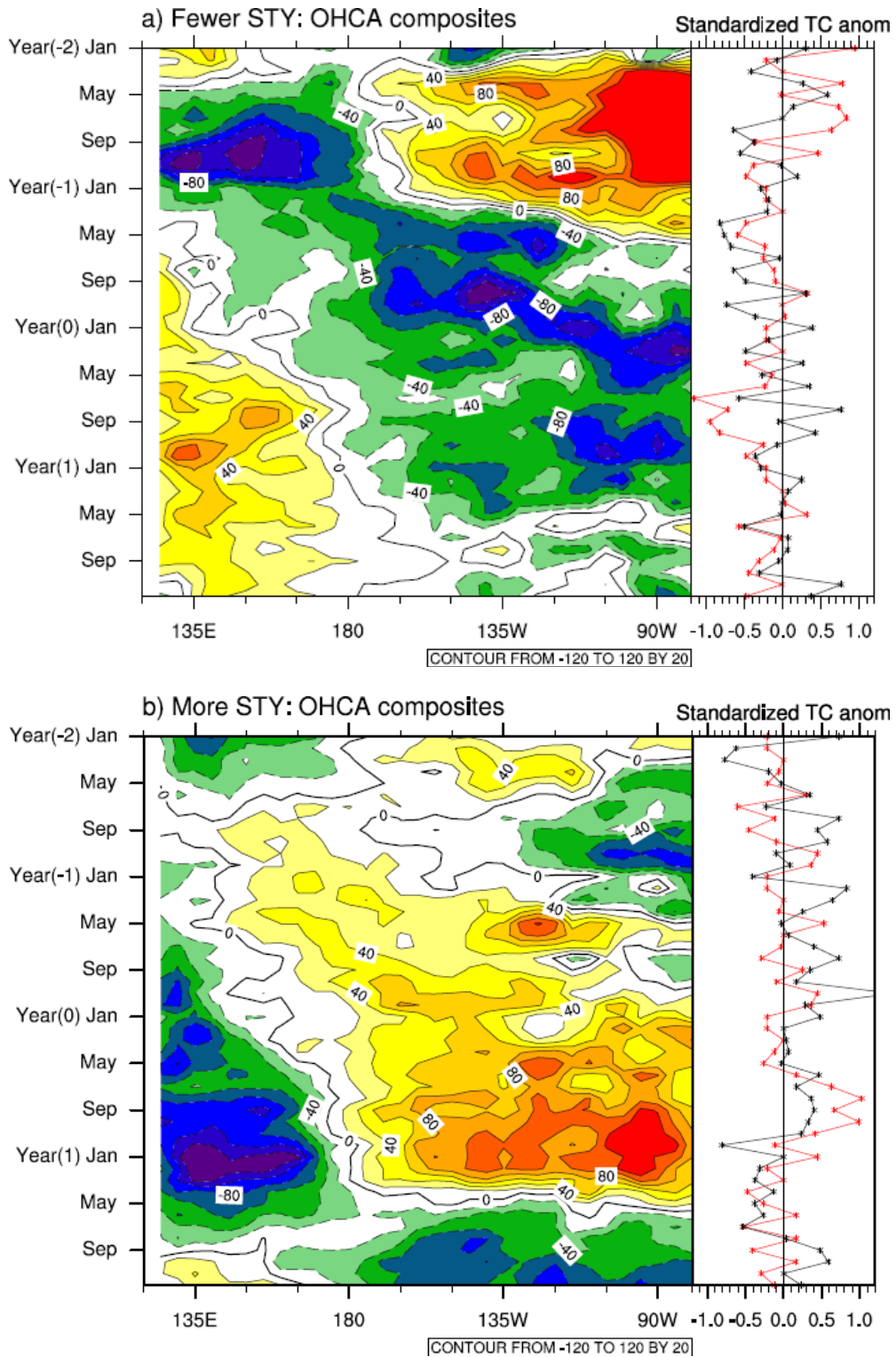


Figure 8: Longitude-time section of OHC anomaly composites (10^8 Jm^{-2}) averaged over 5S–5N for (a) fewer STY years and (b) more STY years, where year 0 refers to the less and more STY years, respectively, and year $-n$ (n) refers to n years before (after) year 0. The red (black) line on the right represents the standardized frequencies of STYs (total TCs) during the composite years.

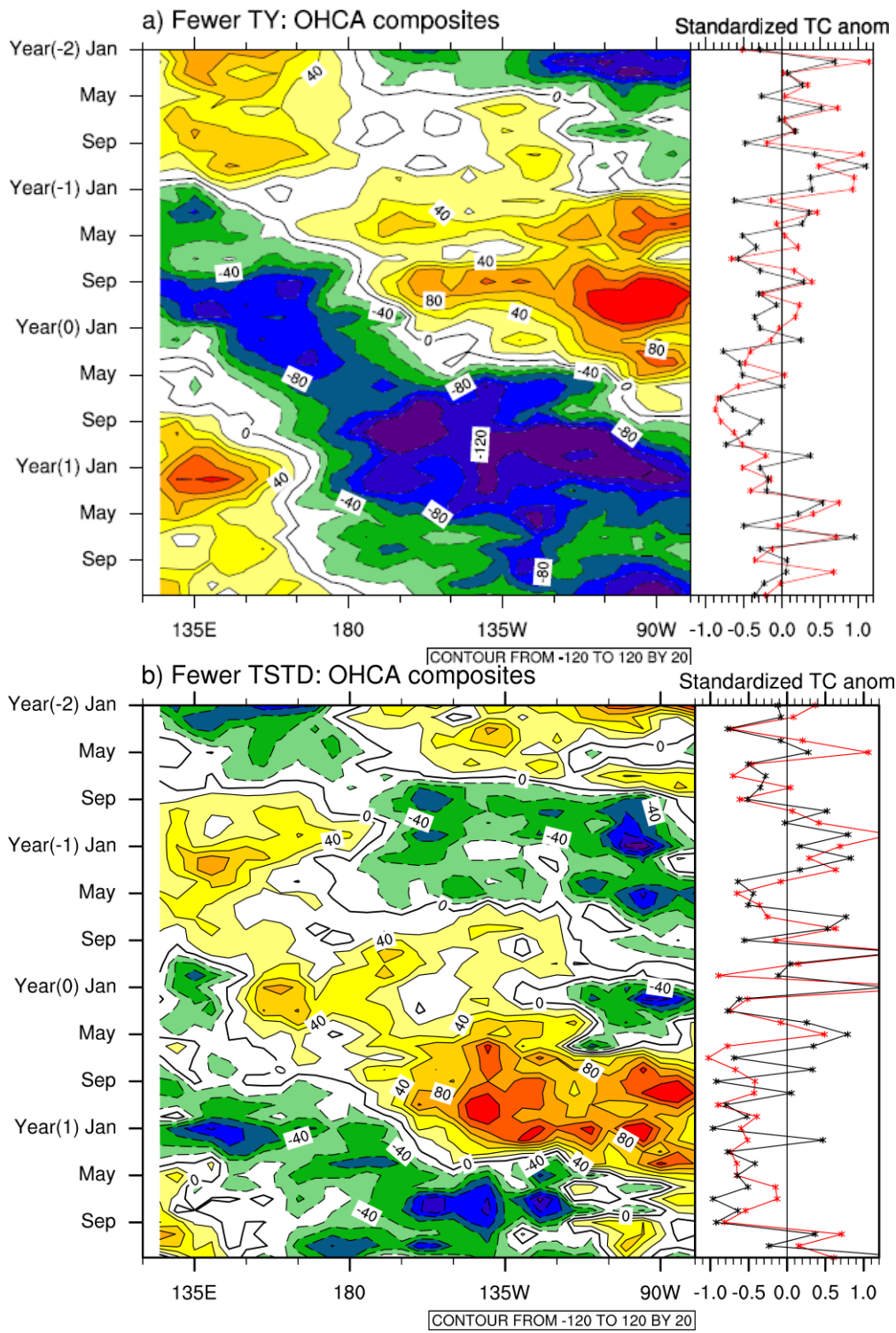
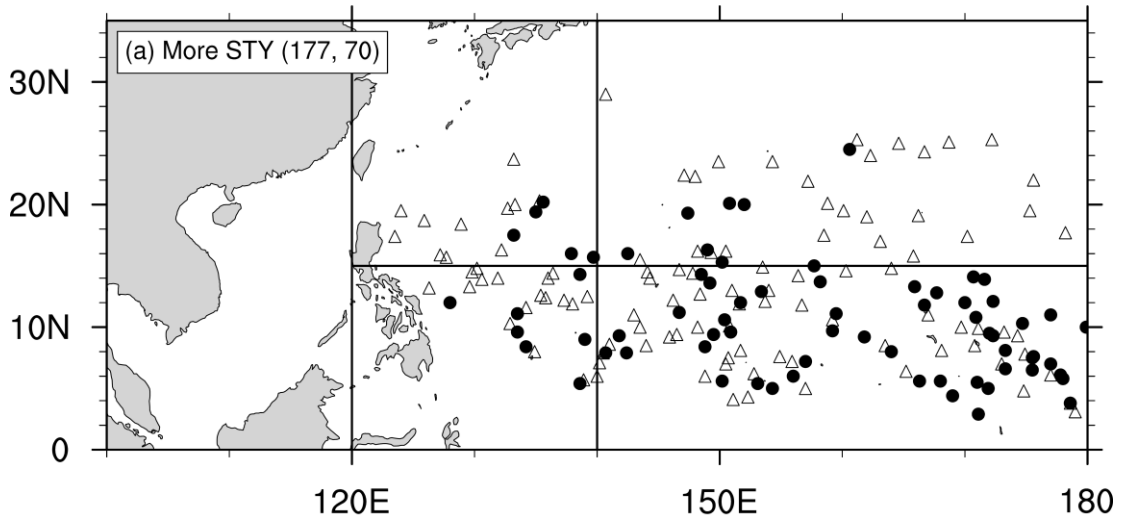


Figure 9: Same as Figure 8, except for (a) fewer TY years and (b) fewer TSTD years. The red line on the right represents the standardized frequencies of TYs and TSTDs, respectively, during the composite years, while the black line denotes the total TC frequency.

Composites: 65, 68, 87, 91, 92, 94, 97, 04



Composites: 66, 74, 78, 85, 99

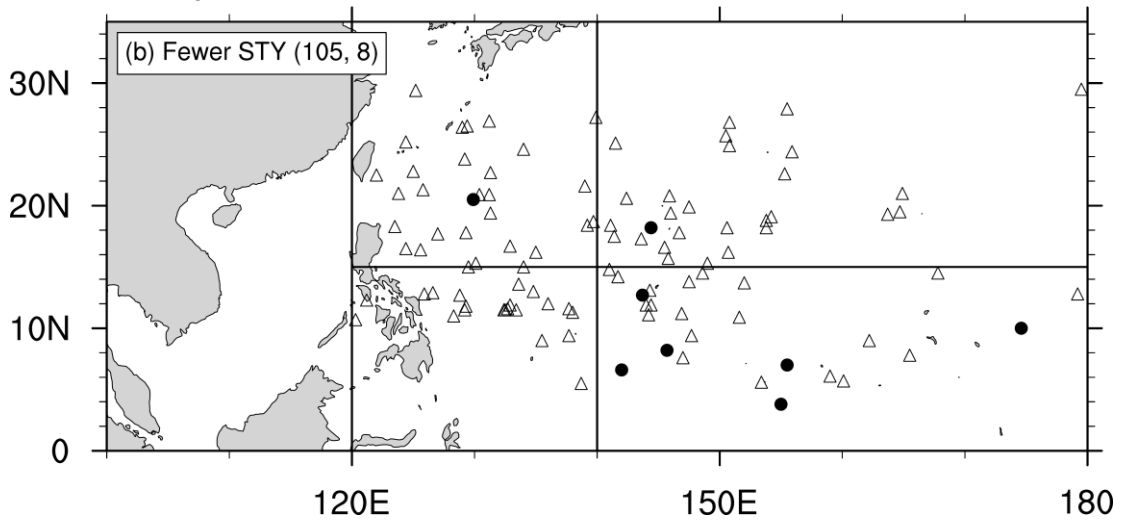
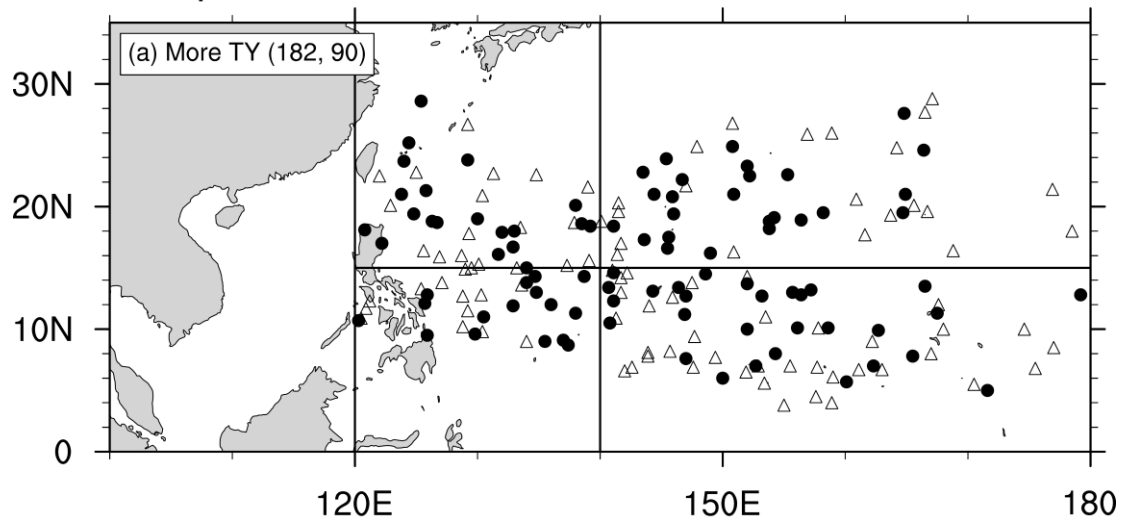


Figure 10: Composite distribution of TCs in (a) more STY and (b) fewer STY years. The black dots represent STY genesis positions while the triangles represent genesis positions other than STY. The numbers within the parentheses indicate the number of total TCs and STYs, respectively, formed during the composite years.

Composites: 67, 71, 74, 78, 85, 90, 93, 01



Composites: 70, 76, 83, 88, 98, 06

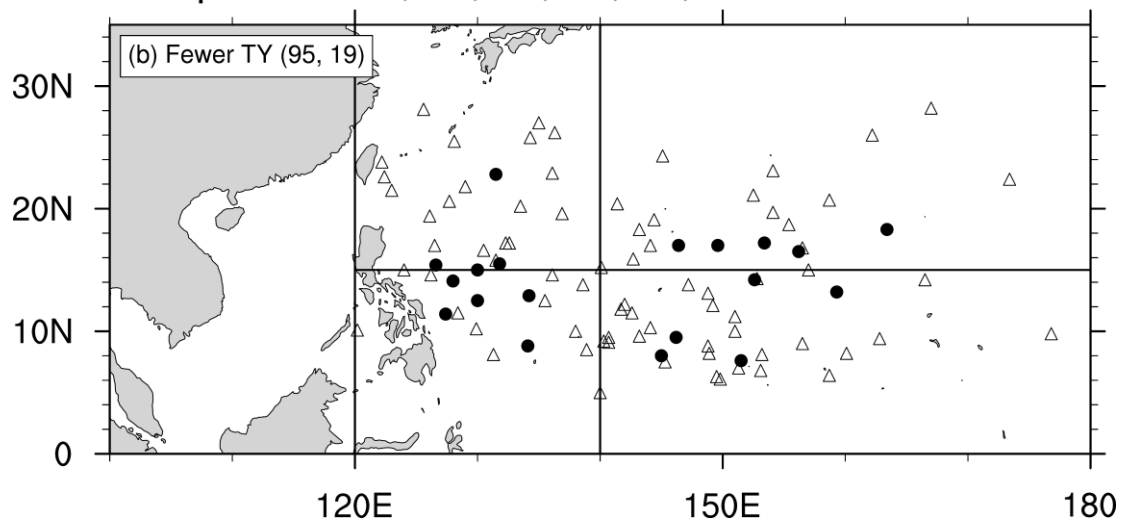
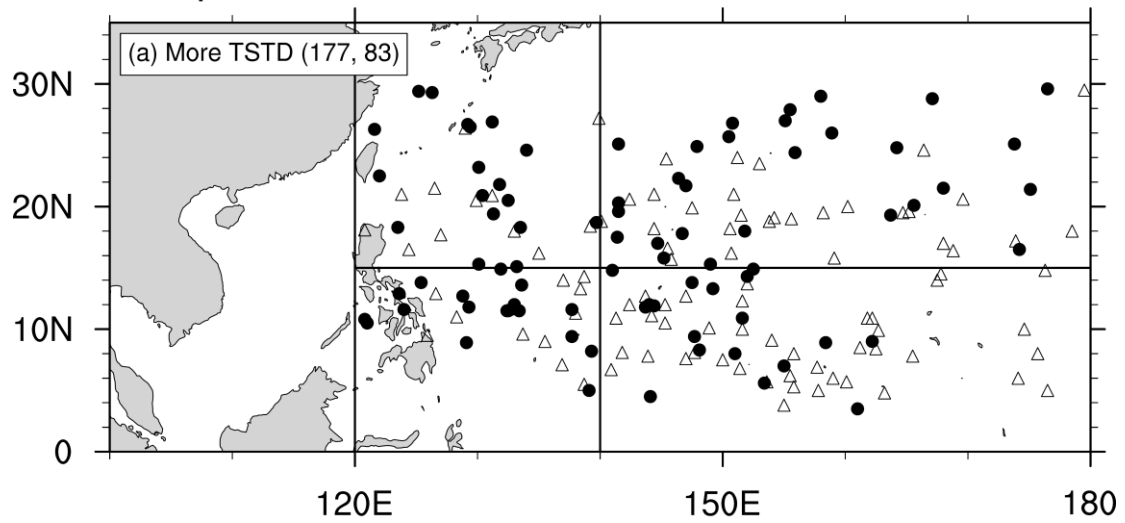


Figure 11: Same as Figure 10, except for (a) more TY and (b) fewer TY years. The black dots represent TY genesis positions while the triangles represent genesis positions other than TY. The numbers within the parentheses indicate the number of total TCs and TYs, respectively, formed during the composite years.

Composites: 66, 67, 78, 89, 95, 96, 99



Composites: 85, 97, 03, 05

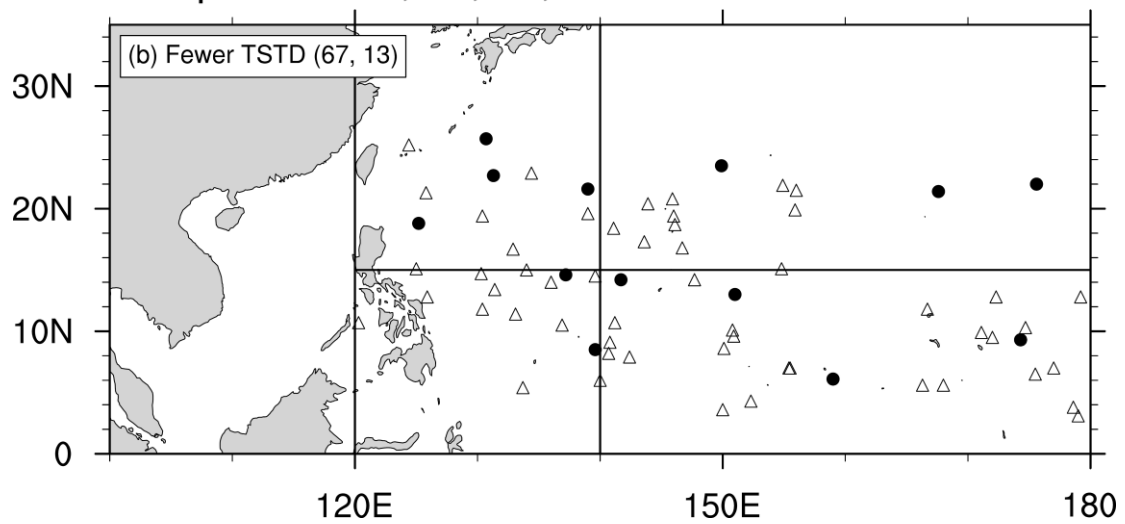


Figure 12: Same as Figure 10, except for (a) more TSTD and (b) fewer TSTD years. The black dots represent TSTD genesis positions while the triangles represent genesis positions other than TSTD. The numbers within the parentheses indicate the number of total TCs and TSTDs, respectively, formed during the composite years.

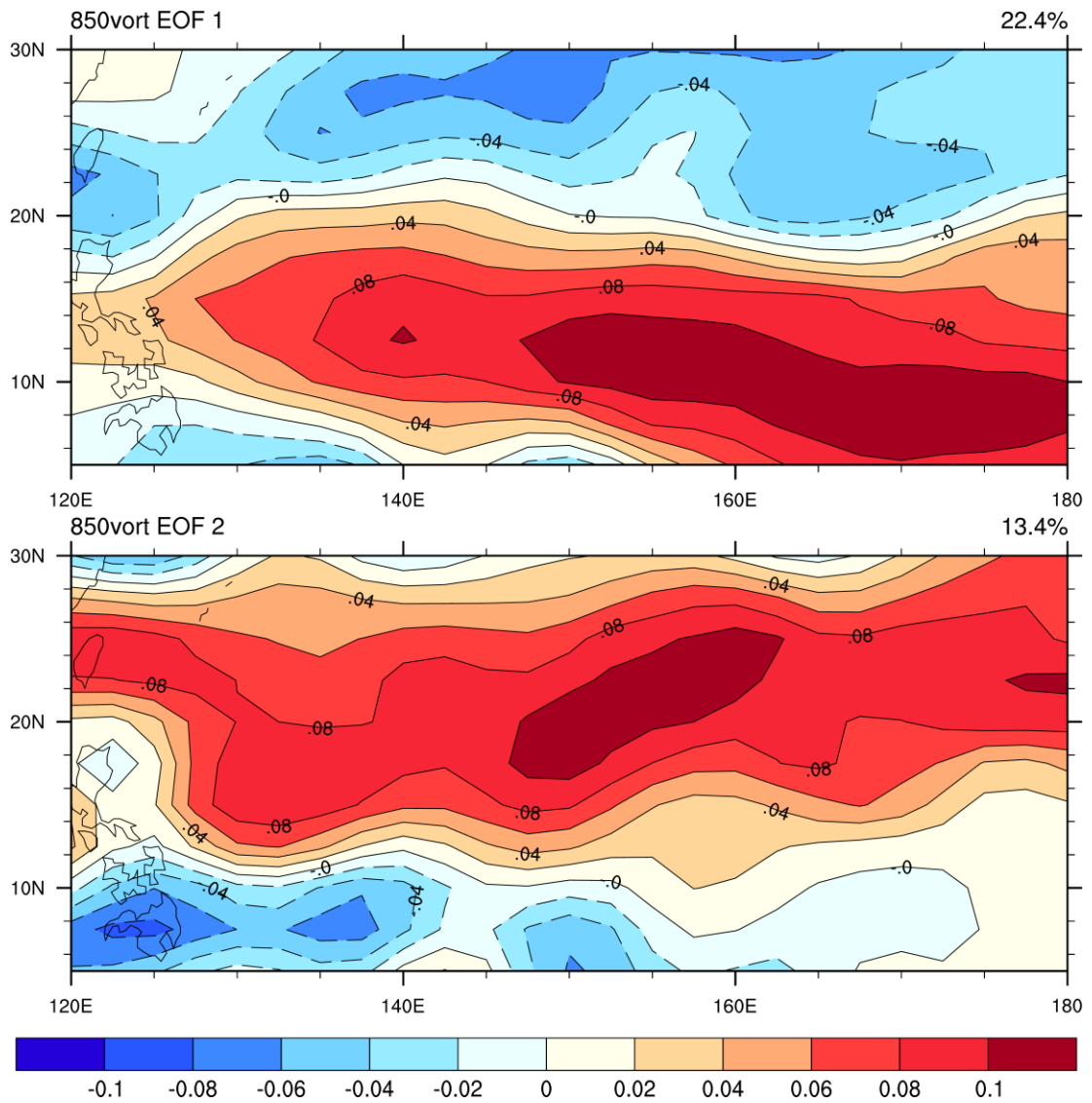


Figure 13: EOF1 (upper panel) and EOF2 (lower panel) of the JASON mean 850 hPa relative vorticity. The sign of the EOF is chosen such that the simultaneous correlation is positive between the PC time series with the PDI. The value in the top right corner indicates the percentage of the total variance explained by each mode.

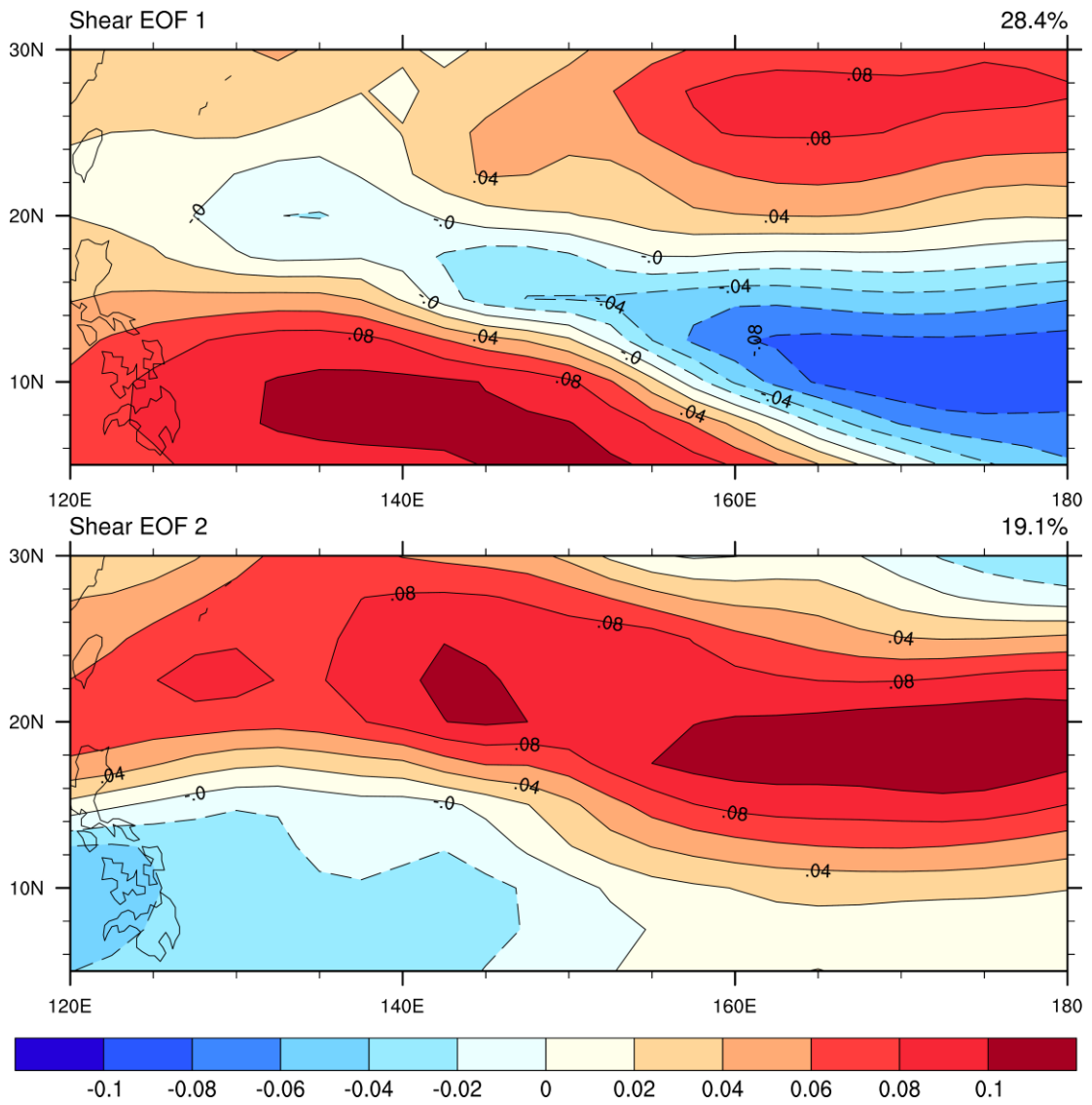


Figure 14: Same as Figure 13, except for the EOF1 (upper panel) and EOF2 (lower panel) of the total vertical wind shear.

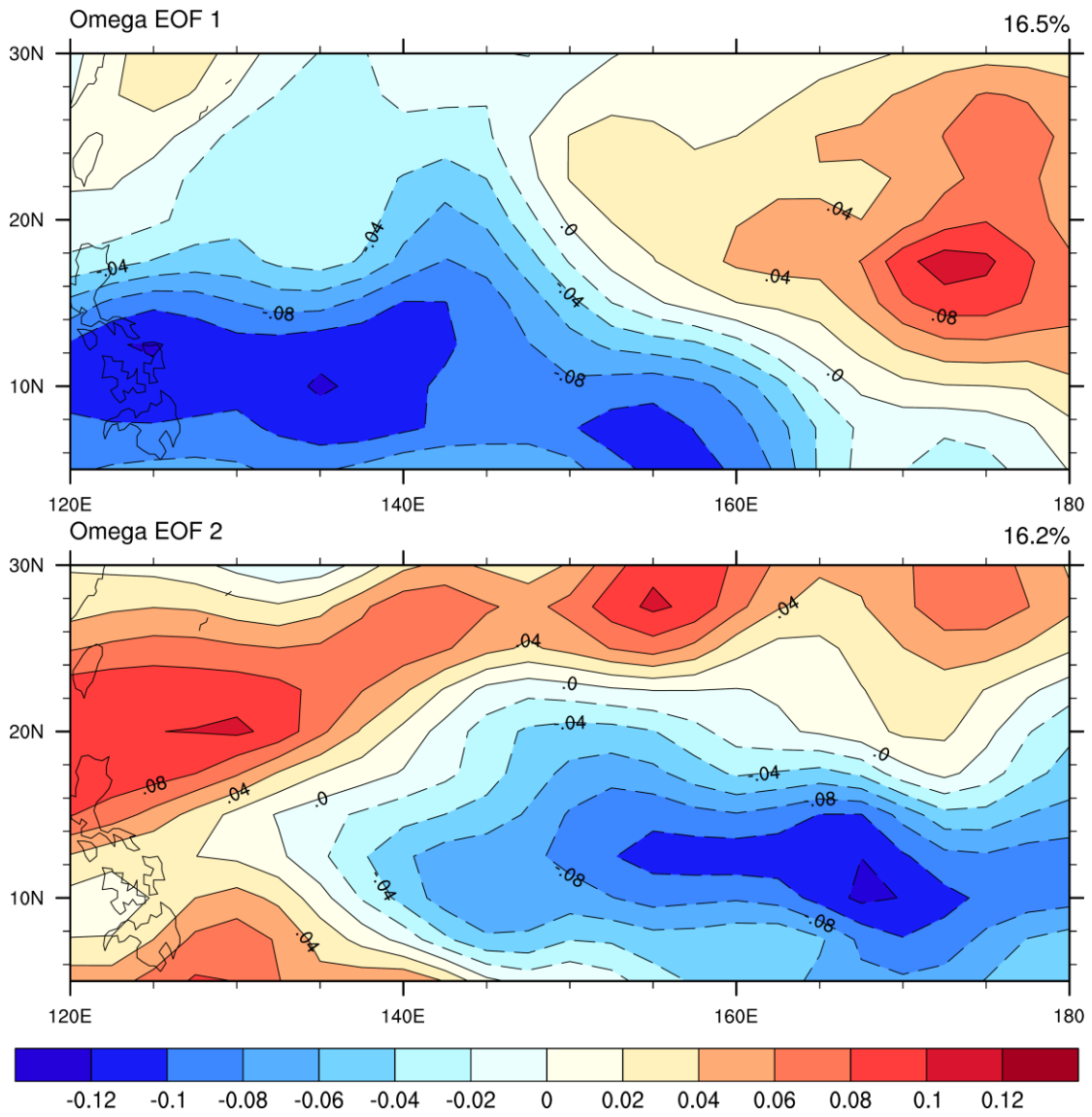


Figure 15: Same as Figure 13, except for the EOF1 (upper panel) and EOF2 (lower panel) of the 500 hPa omega.

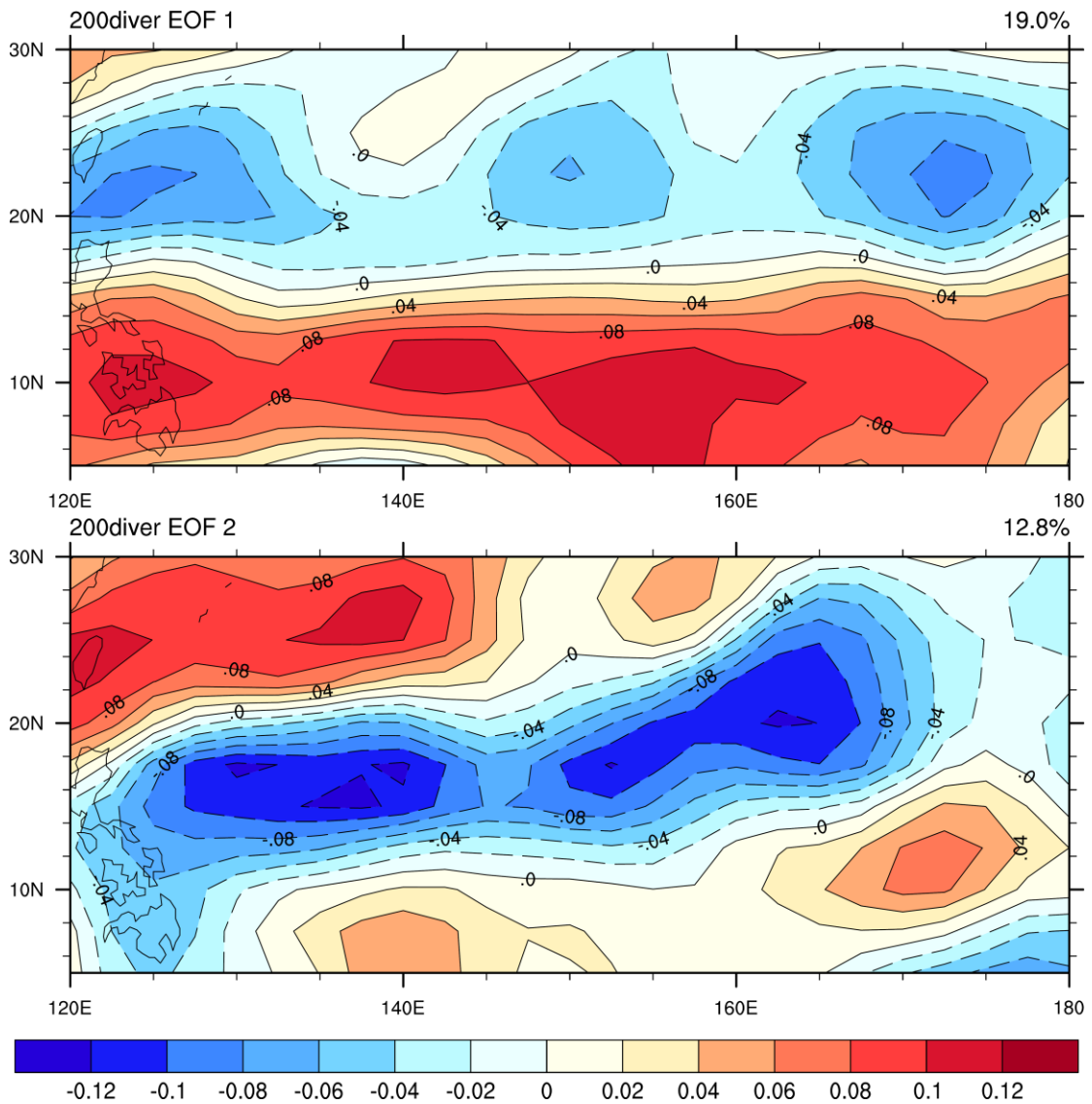


Figure 16: Same as Figure 13, except for the EOF1 (upper panel) and EOF2 (lower panel) of the 200 hPa divergence.

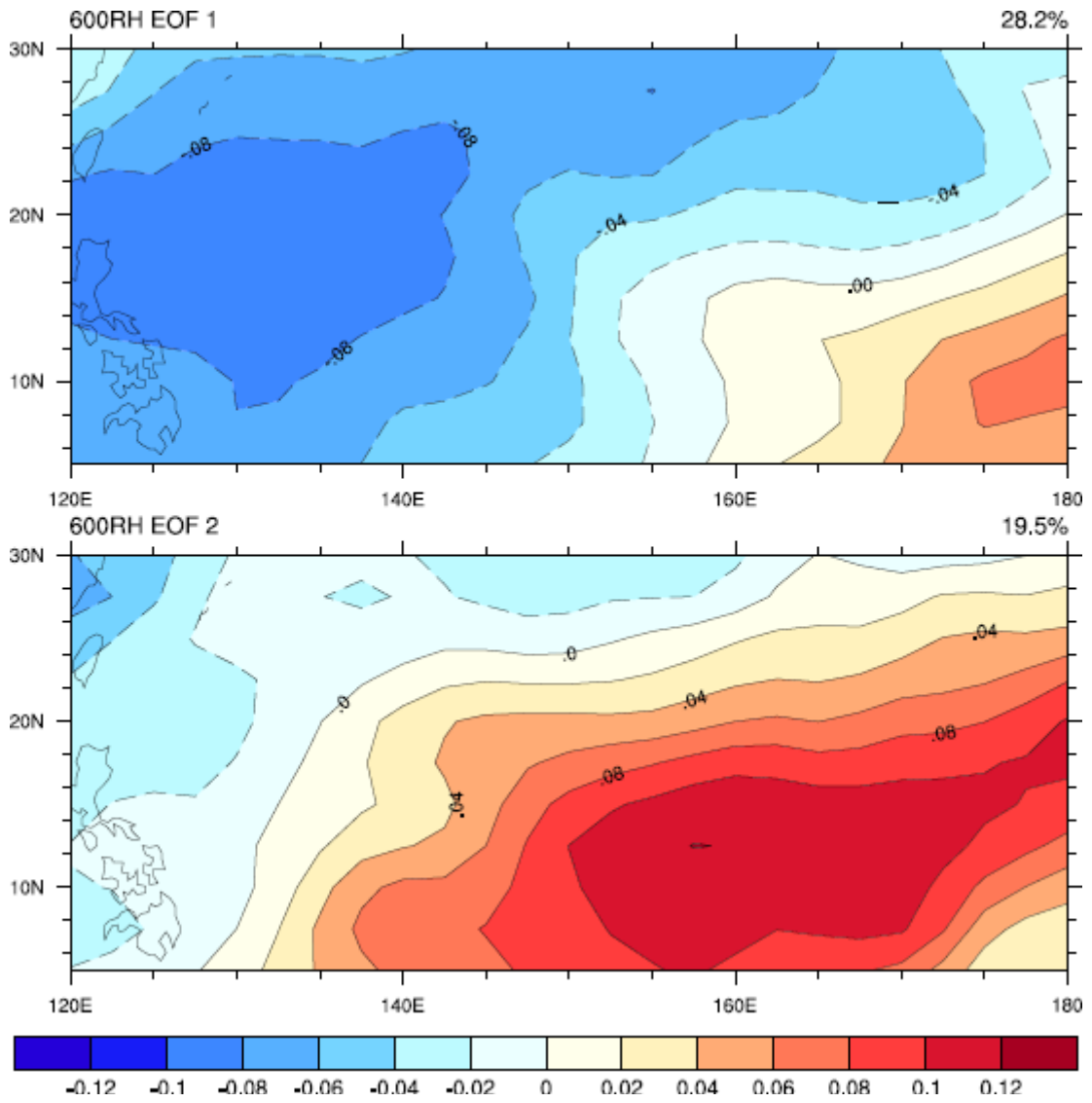


Figure 17: Same as Figure 13, except for the EOF1 (upper panel) and EOF2 (lower panel) of the 600 hPa relative humidity.

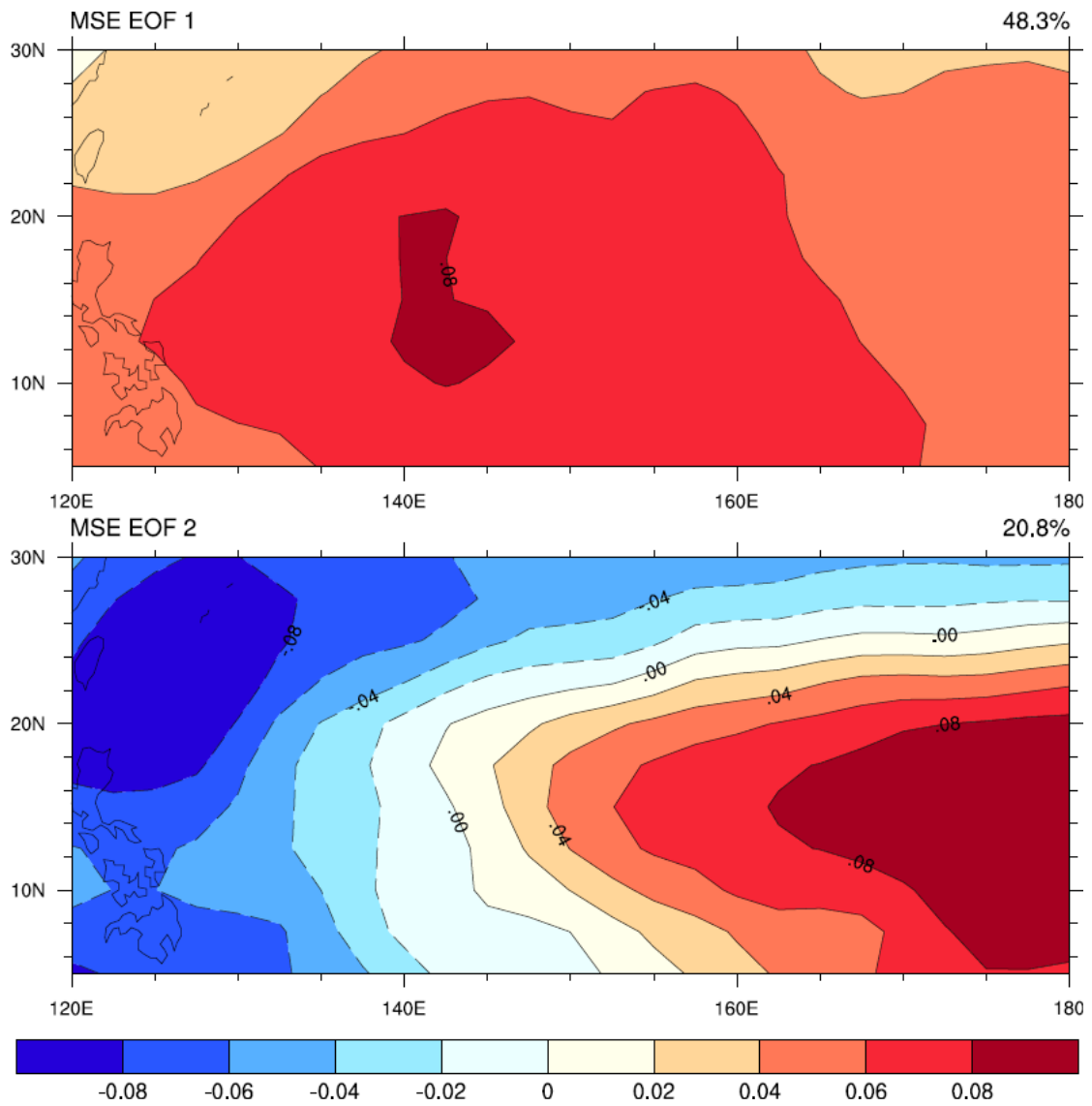


Figure 18: Same as Figure 13, except for the EOF1 (upper panel) and EOF2 (lower panel) of the 1000–500 hPa average moist static energy.

Table 1. Correlation coefficients between frequencies of different TC intensity groups during JASON, obtained by calculating the correlations between the 32-year time series of the frequency of each group of TCs with that of the other groups.

	STY	TY	TDTS
STY	/	-0.23	-0.14
TY	-0.23	/	0.17
TDTS	-0.14	0.17	/

Table 2. More (fewer) TC and STY years selected when the JASON standardized anomalies are greater (less) than or equal to 1 (-1).

More STY years (8 years)	1965, 1968, 1987, 1991, 1992, 1994, 1997, 2004
Fewer STY years (5 years)	1966, 1974, 1978, 1985, 1999
More TY years (8 years)	1967, 1971, 1974, 1978, 1985, 1990, 1993, 2001
Fewer TY years (6 years)	1970, 1976, 1983, 1988, 1998, 2006
More TSTD years (7 years)	1966, 1967, 1978, 1989, 1995, 1996, 1999
Fewer TSTD years (4 years)	1985, 1997, 2003, 2005

Table 3. Accumulated cyclone energy (ACE) and average lifespan of TCs in different years. Bold values indicate the differences between the more and fewer TC years are significant at 95% confidence based on the Student's *t* test.

	ACE per year (10 ⁴ knots)	Average lifespan (days)
More STY years	397	9.8
Fewer STY years	173	6.9
More TY years	251	7.6
Fewer TY years	183	7.0
More TSTD years	251	7.8
Fewer TSTD years	293	9.5
Climatology	256	8.0

Table 4. Correlation coefficients between PC time series of different environmental parameters with the frequencies of different TC groups. Bold values indicate the correlation is significant at least at 90% confidence.

	PC1 with STY	PC2 with STY	PC1 with TY	PC2 with TY	PC1 with TSTD	PC2 with TSTD
850 hPa relative vorticity	0.34 (95%)	0.25	0.076	0.33 (95%)	-0.36 (95%)	0.12
Vertical wind shear	0.31 (95%)	-0.063	0.22	-0.46 (99%)	-0.24	-0.23
500 hPa omega	-0.25	0.41 (99%)	0.053	0.24	-0.078	-0.24
200 hPa divergence	0.22	-0.21	0.012	-0.36 (95%)	-0.16	-0.12
600 hPa relative humidity	0.58 (99%)	0.11	0.028	0.23	-0.14	-0.21
Average moist static energy	-0.019	0.55 (99%)	-0.004	0.13	-0.18	-0.26 (90%)

Table 5. Correlation coefficients between PC time series of different environmental parameters with the PDI at different leads and lags. PC lags (leads) refers to the correlation when the PC time series lags (leads) the PDI by one year. Only values over 90% confidence are shown. Asterisks * (**) denote the correlation between the PDI with the time series of PC1 (PC2) of the parameter.

	PC lags	Simultaneous	PC leads
850 hPa vort	-0.30**	0.85*	0.26**
Total vertical wind shear	/	0.64*	/
500 hPa omega	/	0.71**	/
200 hPa divergence	/	0.71*	/
600 hPa relative humidity	-0.31**	0.52*	/
Moist static energy	/	0.72**	/